Intriguing Effects of Halogen Substitution on the Photophysical Properties of 2,9-(Bis)halo-Substituted Phenanthrolinecopper(I) Complexes

Samantha Brown-Xu, Maria Fumanal, Christophe Gourlaouen, Lea Gimeno, Alessia Quatela, Christine Thobie-Gautier, Errol Blart, Aurélien Planchat, François Riobé, Cyrille Monnereau, et al.

Intriguing effects of halogen substitutions on the photophysical properties of 2,9-(bis)halo substituted phenanthroline-copper(I) complexes

Samantha Brown-Xu,[1] Maria Fumanal,[2] Christophe Gourlaouen,[2] Lea Gimeno,[3] Alessia Quatela,[4] Christine Thobie-Gautier,[3] Errol Blart,[3] Aurélien Planchat,[3] François Riobé,[5] Cyrille Monnereau,[5] Lin X. Chen,[1,6,*] Chantal Daniel,[2,*] Yann Pellegrin[3,*]

[1]Northwestern University, Department of chemistry, Evanston, USA

[2]Laboratoire de Chimie Quantique Institut de Chimie UMR 7177 CNRS-Université de Strasbourg, 4, Rue Blaise Pascal CS 90032, F-67081 Strasbourg Cedex, France.

[3]Université UNAM, CNRS, Chimie Et Interdisciplinarité: Synthèse, Analyse, Modélisation (CEISAM), UMR 6230, 2, rue de la Houssinière – BP 92208, 44322 Nantes Cedex 3, France. E-mail: yann.pellegrin@univ-nantes.fr; Tel: +33 (0)2 76 64 51 74

[4]HORIBA France SAS, Avenue de la Vauve - Passage Jobin Yvon CS 45002 - 91120 Palaiseau – France

[5] ENS de Lyon, CNRS UMR 5182, Université Lyon 1, Laboratoire de Chimie, F69342, Lyon, France

[6] Chemical Sciences and Engineering Division, Argonne National Laboratory, Lemont, Illinois, 60439, USA

Abstract

Three new copper(I) complexes $[Cu(\mathbf{L_X})_2]^+(PF_6^-)$ (where $\mathbf{L_X}$ stands for 2,9-di-halo-1,10-phenanthroline and X = Cl, Br and I) have been synthesized in order to study the impact of halogen substituents tethered in α position of the chelating nitrogen atoms on their physical properties. Photophysical properties of these new complexes (hereafter named **Cu-X**) were characterized both in their ground and excited states. Femtosecond ultrafast spectroscopy revealed that early photo-induced processes are faster for **Cu-I** than for **Cu-Cl** or **Cu-Br**, both showing similar behaviors. Their electronic absorption and electrochemical properties are comparable to benchmark $[Cu(dmp)_2]^+$ (where dmp stands for 2,9-dimethyl-1,10-phenanthroline); furthermore, their optical features were fully reproduced by TD-DFT and *Ab Initio* Molecular Dynamics (AIMD) calculations. All three complexes are luminescent at room temperature, showing that halogen atoms bound to positions 2 and 9 of phenanthroline are sufficiently bulky to prevent strong interactions between the excited Cu complexes and solvent molecules in the coordination sphere. Their behavior in the excited state, more specifically the extent of photoluminescence efficiency and its dependence on temperature, is however strongly dependent on the nature of the halogen. A combination of ultrafast transient absorption spectroscopy, temperature dependent steady state fluorescence spectroscopy and

computational chemistry allows to gain a deeper understanding of the behavior of all three complexes in their excited state.

Keywords: copper(I), phenanthroline, halogen, photoluminescence, thermally activated delayed fluorescence, triplet states.

Introduction

Photochemistry, i.e. the utilization of light (in particular visible light 400-780 nm) as an energy source to trigger processes or to drive photochemical reactions is a very appealing alternative to traditional, thermally activated chemistry. In this context, harvesting and using solar energy as a renewable cheap, efficient and versatile energy source is one of the most obvious benefits of the photochemical approach.[1] The broad range of applications originated in molecular photochemistry gives evidence of the scientific spree associated to the latter: dye-sensitized photo-voltaic devices for solar light conversion into electrical work,[2,3] solar fuels,[4] photosynthesis of commodity chemicals[5] are only a few examples. Photochemical processes relevant to these applications start with light absorption by one or several photosensitizers. One class of photosensitizers ruthenium(II)-polyimine complexes, such as benchmark $[Ru(bpy)_3]^{2+}$, have been extensively studied for these applications.[6] This is fully justified by their impressive properties: photostability, strong absorbance in the visible due to an intense metal to ligand charge transfer band (MLCT), large emission quantum yields combined with long excited state lifetimes and versatile redox states of the metal center affording ubiquitous redox reactivity of the excited state. In addition, they are easy to functionalize and have been used as sensitizers in many photosensitive arrays in all fields of photochemistry briefly mentioned above. Nevertheless, ruthenium complexes (or other heavy metal complexes such as osmium, iridium, or rhodium) are noxious, and the scarcity of this element in the Earth's crust makes it particularly expensive. This justifies the endeavors in the scientific community to substitute ruthenium by more abundant and less toxic elements. Among the huge catalogue of dyes which have been designed to achieve this task, copper(I) complexes of the type $[Cu^{I}(L)_2]^{+}$ (where L is a sterically challenged chelating diimine ligand like 2,9-dimethyl-1,10-phenanthroline, a.k.a. neocuproine or dmp) are very promising.[7-10] They are indeed endowed with an MLCT absorption band in the visible within the same range than $[Ru(bpy)_3]^{2+}$, they are photoluminescent (*via* a thermally activated delayed fluorescence process, TADF),[11] and strongly photo-reductant.[8,9,12,13] Although the lability of the coordination sphere has long been an issue to isolate multi-functional species (e.g. dyads or triads), progresses have been made

towards the synthesis of complex photosensitive arrays proving that copper(I) complexes could exhibit virtually the same versatility as ruthenium(II) complexes.[3,14]

Since the discovery of their near IR (NIR) photoluminescence by McMillin et al. in 1980,[7] their photophysical properties have been regularly improved; in particular, the luminescence quantum yield has evolved from $2.4x10^{-4}$ to $5.6x10^{-2}$, and the emission lifetimes from 90 ns to more than 3 µs.[10,15] Those improvements are grounded in the progressive increase of the steric hindrance around chelating nitrogen atoms of the diimine ligand.[16,17] There has been indeed an extensive work on the impact of bulky substituents around the copper(I) coordination sphere, leading to an understanding of the photo-induced processes within such copper complexes. Briefly, $[Cu^{I}(L)_2]^+$ complexes undergo an internal charge transfer upon MLCT excitation following the equation below:

$$[Cu^{I}(L)_2]^+ + hv \rightarrow [Cu^{II}(L)(L^{\bullet-})]^+$$

When the complex is excited, the pseudo-tetrahedral (D_{2d}) copper(I) $3d^{10}$ is transiently oxidized into copper(II) $3d^9$ via the metal-to-ligand-charge-transfer (MLCT) transition where an electron from the Cu center is transferred to a ligand centered π* orbital. Consequently, the Jahn-Teller distortion occurs which flattens the tetrahedral copper(I) towards to square planar copper(II) (D_2), enabling an access for the coordinating solvent molecules to interact with the copper(II) center, and causing very fast quenching of the excited state. This deactivation is due to the strong stabilization of the lowest excited states *via* the flattening and Cu (II)*-solvent interactions enabled by this flattening, leading to non-radiative decay by virtue of the energy gap law for radiationless transitions.[18]

Various bulky substituents R positioned at different positions of phenanthroline ligands have been used to alter the excited state behaviors, especially to prolong lifetimes and enhance luminescence quantum yields. Among them, the most frequently explored are linear and ramified alkyl chains, or aromatic groups at the 2,9 positions because they are quite easy attached to the phenanthroline core and have been shown to hinder the excited state quenching mechanism as aforementioned.[17,19] The impact of the steric bulk on the luminescence properties has been highlighted in a number of landmark articles,[8,10,12,20] such as the works of Castellano and McCusker on $[Cu(dsbp)_2]^+$ and $[Cu(ipp)_2]^+$ complexes (where dsbp and ipp respectively stand for di-secbutyl-1,10-phenanthroline and di-isopropyl-1,10-phenanthroline),[21,22] Burstyn[15] and Chen[23] on $[Cu(dtbp)_2]^+$ (where dtbp stands for 2,9-di-terbutyl-1,10-phenanthroline), the latter holding a very high emission quantum yield and the longest lifetime ever reported for a homoleptic copper(I)-bis(diimine) complex in solution ($5.6x10^{-2}$ and 3.26 µs respectively).

The great majority of the photophysical studies on copper(I) complexes focuses on the steric features of alkyl and aryl substituents at 2,9-positions, mainly shielding the copper center from the solvent. Less is known about the impact of electronic effects of these groups although a great many structures have already been exposed in the literature (e.g. alkoxy[24,25] and thio-alkoxy,[26] primary and secondary amines,[27] phosphine and phosphine oxide,[28] amide,[29] imidazole and imidazolium,[30] etc.). Let us nevertheless mention the case of a luminescent heteroleptic copper(I) complex where the metal ion is coordinated by the famous diphosphine xantphos and bipyridine bearing chlorine and bromine atoms in α of the chelating nitrogens, for OLED applications.[31]

Within this frame, we have carried out studies on the physical properties of $[Cu(\mathbf{L_X})]_2^+$ complexes where $\mathbf{L_X}$ stands for 2,9-dichloro/dibromo/diiodo-phenanthrolines $\mathbf{L_{Cl}}$, $\mathbf{L_{Br}}$ and $\mathbf{L_I}$ respectively (figure 1). Monitoring the properties of those complexes by simply varying the halogen substituent allows to appreciate the impact of gradually changing the electron-withdrawing character of the phenanthroline ligand without altering too significantly the structure of the latter nor the complex. We were interested in exploring if the steric bulk imposed by halogen atoms was sufficient to promote excited state properties of the corresponding copper(I) complexes and what is the impact of the electron withdrawing character of halogen atoms, opposing to electron donating alkyl groups.

In this contribution, we report the successful observation of a significant photoluminescence at room temperature in dichloromethane from **Cu-Cl**, **Cu-Br** and **Cu-I**. The impact of the halogen substitution on the electronic properties of the complexes in the ground and excited states is discussed and rationalized thanks to joint experimental and theoretical studies. We show that a thermally activated delayed fluorescence process (TADF) is at stake for **Cu-Cl** and **Cu-Br**. Meanwhile, an unexpected opposite evolution is monitored in the case of **Cu-I** which features the best emission quantum yield and longest excited state lifetime. These features are interpreted on the basis of the calculated potential energy profiles connecting the fully optimized structures of the complexes in the electronic excited states under various symmetry constraints.

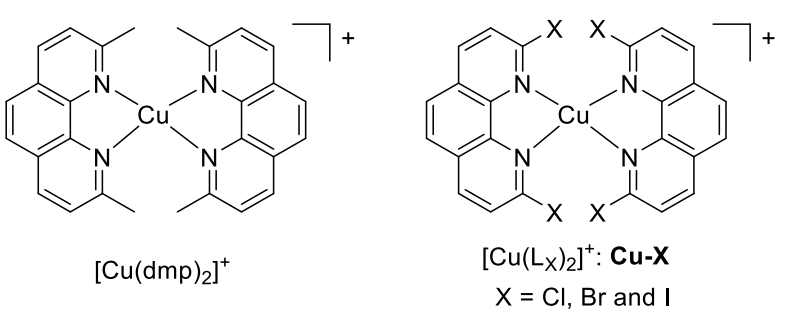

Figure 1. Structures of the complexes presented in this study.

Results and Discussions

Molecular Structures

The syntheses of complexes **Cu-Cl**, **Cu-Br** and **Cu-I** were performed at room temperature by mixing one equivalent of $Cu(CH_3CN)_4PF_6$ with two equivalents of the corresponding 2,9-dihalo-1,10-phenanthroline ligand $\mathbf{L_X}$ in dichloromethane, under an argon atmosphere. Bright orange solutions were obtained in all three cases. ^{1}H-NMR and high resolution mass spectra confirmed the expected structures. Slow diffusion of diethyl ether in dichloromethane solutions of **Cu-Cl** afforded mono-crystals which were suitable for an X-ray structure resolution. Despite repeated trials with various conditions, monocrystals of **Cu-Br** or **Cu-I** could not be obtained, partly due to the poor solubility of the latter in dichloromethane and instability in other solvents (see below). The structure of **Cu-Cl** is presented in figure 2. Bond lengths and angles of interest are reported in table 1, all values are in agreement with previously published structures for symmetrical homoleptic copper(I)-bis(diimine) complexes. **Cu-Cl** exhibits a distorted tetrahedral geometry, with an angle of ca. 72° between phenanthroline planes. The phenanthroline-copper CuN_2 moieties are not equivalent, one being rather symmetrical (Cu-N1B = 2.051 Å and Cu-N2B = 2.041 Å) while the other is strongly distorted (Cu-N1A = 2.058 Å and Cu-N2A = 2.027 Å). This is likely due to crystal packing forces; no such behavior was monitored in solution as proven by the NMR data which are in favor of a completely symmetrical structure.

Distances (Å)				Angle between phen planes (deg)					
Cu-N1A	Cu-N2A	Cu-N1B	Cu-N2B	N1A-Cu-N2A	N1B-Cu-N1A	N1A-Cu-N2B	N1B-Cu-N2A	N2A-Cu-N2B	N1B-Cu-N2B
2.058 (4)	2.027 (3)	2.051 (4)	2.041 (4)	81.87 (14)	109.72 (14)	128.67 (15)	134.04 (14)	126.66 (14)	81.43 (14)

Table 1. Bond lengths and angles of interest in the structure of **Cu-Cl**

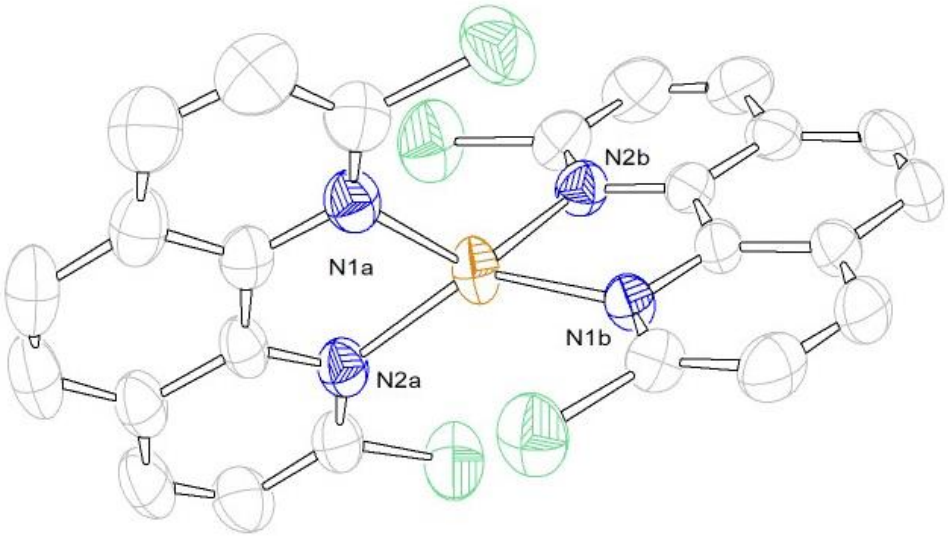

Figure 2. Perspective view of complex **Cu-Cl** (50% probability ellipsoids). H atoms are omitted for clarity.

Electronic absorption spectroscopy

UV-Vis spectra of complexes **Cu-X** were recorded in dichloromethane solutions and are presented in figure 3. Associated relevant data are gathered in table 2. All three complexes feature intense absorption bands around 300 nm which are associated to intraligand π-π* transitions, and a broad band spanning from 400 to 600 nm, classically assigned to the MLCT transitions that are responsible for their bright orange color. The spectra features are substantially dependent on the nature of the halogen X tethered to the 2,9 positions of the phenanthroline ligands. The heavier X, the more red-shifted the absorption maxima wavelengths λ_{abs} (table 2). It is worth noting that, while the effect remains limited when going from Cl to Br, the extent of red-shifting is much more pronounced upon substitution with I underlying a particular influence of the latter on the electronic structure of the complex. The fact that the MLCT is a combination of several transitions to high lying singlet states makes it difficult to expose a simple explanation of the observed trend. Yet, the electron-withdrawing effects (EWE) of X (which decreases when scrolling down the halogen column from Cl to I) has an obvious impact on the orbitals involved in the MLCT transition manifold, which was accurately reproduced by TD-DFT calculations (see calculation section below).

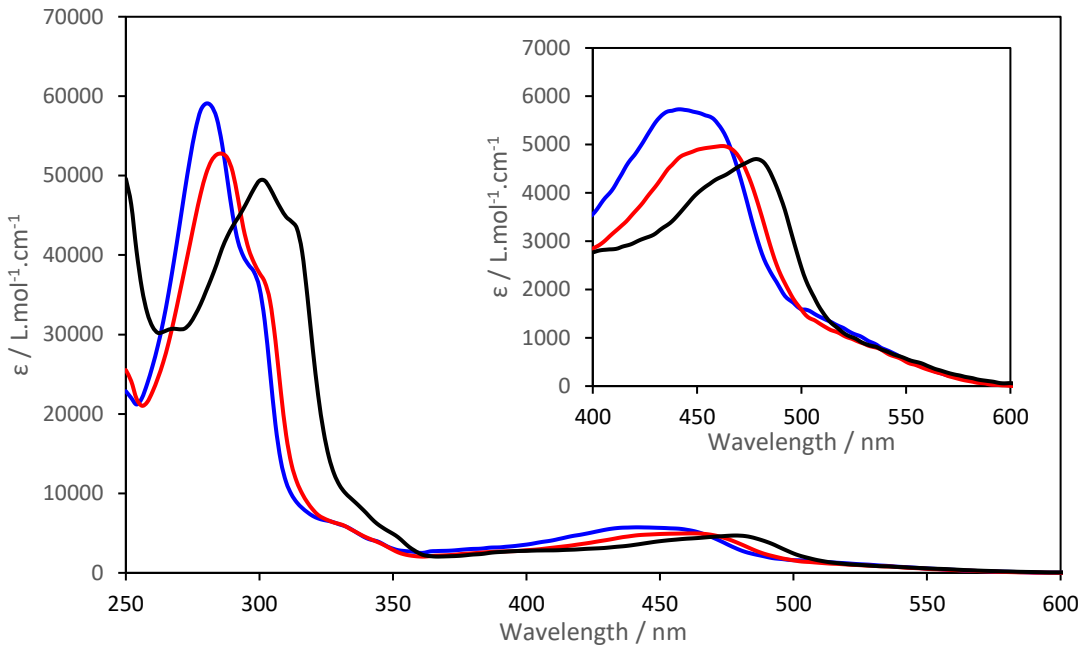

Figure 3. Absorption spectra of complexes **Cu-Cl** (blue line), **Cu-Br** (red line) and **Cu-I** (black line) recorded in dichloromethane. Inset: focus on the MLCT transitions.

The MLCT of **Cu-Cl**, **Cu-Br** and **Cu-I** collapsed when aliquots of acetonitrile were added in a dichloromethane solution of the latter complexes (figures S1), revealing a significant instability of those complexes in presence of coordinating competitors. While the intensity of the MLCT decreases, a broad band rises at ca. 370 nm; the overall shape of the spectra is consistent with $[CuL_X(CH_3CN)_n]^+$.[32] This is likely due to the decreased σ-donating power of the phenanthroline cavity owing to EWE from halogen substituents. Incidentally, **Cu-I** is more stable *vs.* ligand exchange with CH_3CN than **Cu-Cl** and **Cu-Br** (figure S2), in line with the stronger electron-withdrawing effects of chlorine and bromine compared to iodine.

	λ_{abs} / nm (ε / L.mol^{-1}.cm^{-1})	λ_{em} / nm	Φ_{em} x 10^4	τ_{em} (ns)[a]	k_r (s^{-1})	k_{nr} (s^{-1})	E_{ox}[b]	E_{red}[c]
Cu-Cl	440 (5730)	715	2.4	62.70 (±0.34)	$3.8x10^3$	$16x10^6$	1.05	-1.41
Cu-Br	460 (4970)	700	8.1	105.70 (±0.40)	$7.7x10^3$	$9.5x10^6$	1.20	-1.32
Cu-I	480 (4700)	700	8.8	109.60 (±0.28)	$8.0x10^3$	$9.1x10^6$	1.26	-1.28
$Cu(dmp)_2^{+}$[17]	454 (7800)	730	2.4	85	$2.8x10^3$	$11x10^6$	0.95	-

Table 2. UV-Vis, emission and electrochemical data for complexes **Cu-Cl**, **Cu-Br** and **Cu-I** in dichloromethane. [a]Degassed dichloromethane solutions. [b]Half wave potentials. [c]Irreversible process, peak potential. Sweep rate for electrochemical measurements = 100 mV.s^{-1}. All data recorded at room temperature.

Electrochemistry

Cyclic voltammograms were recorded for the three complexes in dichloromethane in presence of 0.1 M tetra-n-butylammonium hexafluorophosphate as a supporting electrolyte. A platinum working electrode was used. All potentials are quoted *vs.* the saturated calomel reference electrode (SCE) and reported in table 2; the voltammograms are given in figure S3. At first sight, the three complexes display similar electrochemical behaviors: one reversible oxidation process corresponding to the copper centered oxidation and one irreversible reduction event we assigned to the addition of an extra electron on $\mathbf{L_X}$. Both potentials depend on the nature of X. The oxidation potentials are shifted to more positive values from X = Cl to X = I. A similar observation has been made in a previous work by Orti, Housecroft et al.[31] This is in contrast with the trend one could expect by considering the electron withdrawing effects from halogen atoms, decreasing in the order Cl > Br > I. On the other hand, steric effects are known to strongly affect the redox potentials of copper(I) complexes: the bulkier the R substituents, the closer to a rigid tetrahedral geometry the coordination sphere and the more stabilized the copper(I) ion, yielding a more anodic Cu(II)/Cu(I) potential.[10,15,17] Here, we note that the oxidation potentials increase indeed with the size of the halogen (from Cl to I), which tend to indicate that steric constraints overwhelm electronic effects. These results show the difficulty to find a simple rationale when both electronic and steric effects are involved.[33]

Reduction of copper-phenanthroline complexes is usually a very cathodic process (below -1.6 V vs. SCE),[34,35] independent of the steric bulk around the Cu(I) ion, since the reduction is centered on the phenanthroline ligand. The **Cu-X** complexes are among the few examples of copper-bis(phenanthroline) complexes[34,36] which can be reduced within the electrochemical window of dichloromethane. The reduction processes are irreversible (even at 1 V/s sweep rate) regardless the nature of X, making it risky to discuss the evolution of the peak potentials. This irreversibility contrasts with common $[CuL_2]^+$ complexes, where aliphatic chains or aromatic groups are tethered in positions 2 and 9 of the phenanthroline. Interestingly, calculations reveal there is no contribution of the halogen atoms to the electronic density of the LUMOs, regardless X (figure S4). Cleavage of the C-X bond upon reduction is thus unlikely. Preliminary reductive bulk electrolysis of a solution of **Cu-Br** in a dichloromethane electrolyte at a controlled potential of -1.36 V vs. SCE yielded a colorless solution, proving that the $[Cu(L_X)_2]^+$ coordination cage fell apart upon reduction. The UV-Vis spectrum of the resulting solution presents the features of pure $\mathbf{L_{Br}}$ (figure S5) and the electrolyzed solution promptly turned orange upon addition of $Cu(CH_3CN)_4PF_6$. We thus conclude that reduction of the complex is quickly followed by decoordination of copper(I) owing to the lesser stability of **Cu-X** compounds as compared to aliphatic substituted ones.

Steady state luminescence

The luminescence properties of the **Cu-X** complexes were evaluated by steady state fluorescence spectroscopy at room temperature. The spectra are presented in figure 4 and relevant data (maximum emission wavelengths, emission quantum yields) are gathered in table 2. All complexes are luminescent, proving that halogen substituents are sufficient to prevent to a certain extent the photo-induced flattening and solvent-solute interactions of the coordination cage. Emission spectra fall within the same spectral range for all complexes, with broad emission bands and maxima comprised between ca. 700 and 715 nm as commonly observed for copper(I)-bis(diimine) complexes. We estimated the energy of the lowest excited state by the tangent method,[37] and all three complexes displayed a value of ca. 2.1 eV, in line with TD-DFT calculations (see below).

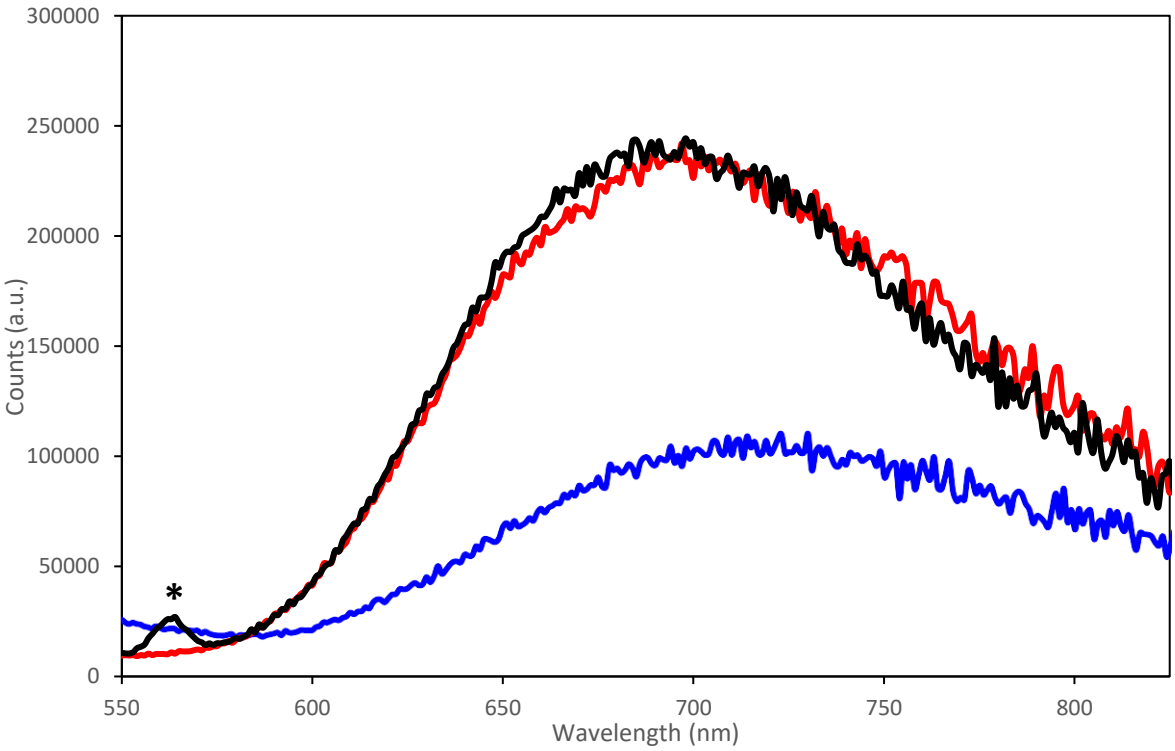

Figure 4. Steady state emission spectra for complexes **Cu-Cl** (blue), **Cu-Br** (red) and **Cu-I** (black) in absorption matched (OD = 0.1 a.u. at maximum absorption wavelength) dichloromethane solutions, after excitation at 440, 460 and 480 nm respectively. *Corresponds to Raman signal of CH_2Cl_2 upon excitation at 480 nm.

At first glance, **Cu-Br** and **Cu-I** display substantially higher luminescence quantum yields compared to **Cu-Cl**, as well as blue-shifted maximum emission wavelengths. Those experimental results could be preliminarily explained by an increased steric hindrance within the series chlorine, bromine and iodine since the bulkier the substituents in positions 2 and 9 of the phenanthroline, the more intense the luminescence. Nevertheless, the electrochemical

study (see above) revealed that electronic effects should not be ignored to rationalize the properties of the **Cu-X** complexes in their ground state; their implication in the excited states behavior is therefore more than likely. This is evidenced by the higher emission quantum yield of **Cu-I** *vs.* $[Cu(dmp)_2]^+$ which is difficult to rationalize only on steric grounds.

Radiative (k_r) and non-radiative (k_{nr}) constants could be retrieved from the steady state and time resolved emission data (table 2), using equations $k_r = \Phi_{em}/\tau_{em}$ and $k_r + k_{nr} = 1/\tau_{em}$. As usual with copper(I)-bis(diimine) complexes, k_{nr} is three to four orders of magnitude larger than k_r, justifying their modest emission quantum yields. **Cu-Br** and **Cu-I** feature similar rate values at room temperature. Interestingly, **Cu-Cl** is endowed with a larger k_r than $Cu(dmp)_2^+$ but exhibits the largest k_{nr} in the whole series signifying that particularly effective non-radiative deactivation channels are open in this case (see below).

Temperature dependence of steady-state emission spectra

In order to investigate the photophysical behavior of the three complexes, we monitored their luminescence properties as a function of temperature. Usually, copper(I)-bis(diimine) and heteroleptic copper(I)-(bisphosphine)(diimine) complexes feature a TADF mechanism;[11] briefly, the gap between the lowest singlet and triplet states (S_1 and T_1) is sufficiently small to allow reverse intersystem crossing (rISC) activated by thermal motions at room temperature.[38] As such, when the temperature is decreased, the rISC is less likely and the emission spectra is more and more dominated by the longer lived (but weaker) triplet based emission.[11,21,39] As a consequence, the luminescence intensity collapses when the temperature decreases and the emission maximum is red-shifted, as monitored for mainstream complexes such as $[Cu(dmp)_2]^+$[11] or $[Cu(ipp)_2]^+$ (ipp = 2,9-diisopropyl-1,10-phenanthroline).[21] The luminescence spectra of **Cu-Cl** and **Cu-Br** follow the same trend and both complexes can be considered as TADF emitters. On the other hand, **Cu-I** features the opposite behavior (figure 5): the luminescence intensity increases as the temperature decreases. At the same time, the luminescence spectra is red-shifted by ca. 20 nm (figure S6). All those results tend to prove that in the case of **Cu-I**, the emission originating from the singlet deactivation is a less efficient process than the luminescence from the triplet state ($\Phi_S < \Phi_T$ in the case of **Cu-I**). This behavior is unexpected, and strikingly contrasts with the trend usually monitored for copper(I)-diimine complexes. It is however unambiguous and furthermore corroborated by the calculations performed on the series (see below).

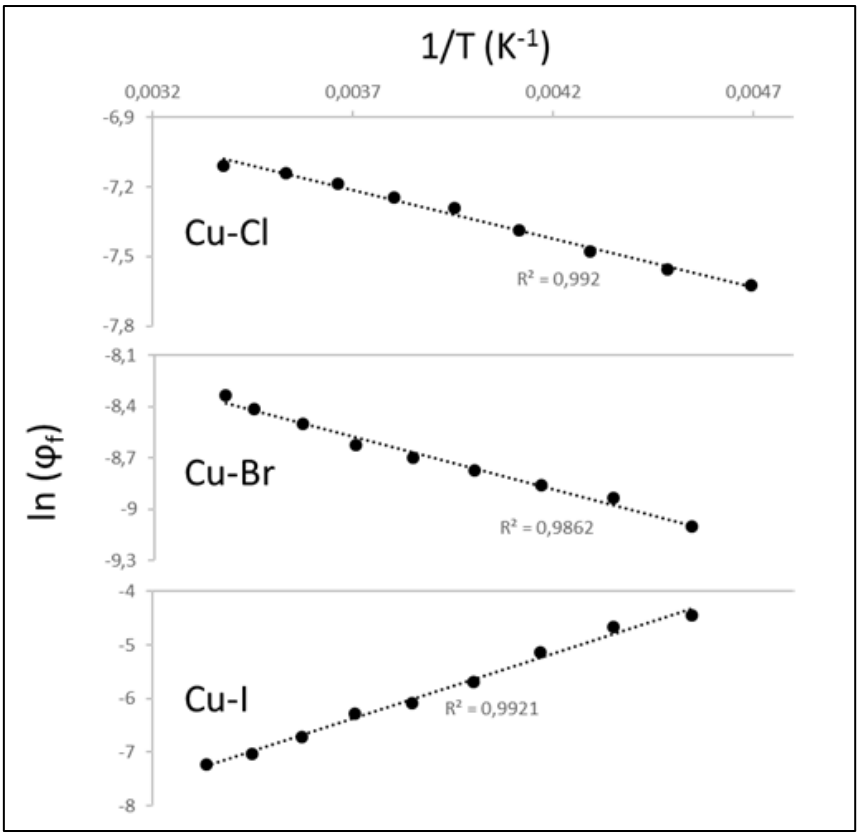

Figure 5. Arrhenius plot $\ln(\varphi_{em}) = f(1/T)$ (black circles) for **Cu-Cl**, **Cu-Br** and **Cu-I** in the range 210-310K. Dotted lines: linear regression.

Remarkably, the fact that luminescence efficiencies of the three complexes follow an Arrhenius law when plotted against temperature suggests that singlet-triplet equilibrium is in the three cases at the origin of the observed trend, although it translates in two opposites effects: facilitating the rISC process by thermal effects favors emission in **Cu-Cl** and **Cu-Br**, where the latter originates mainly from the singlet state (at higher energy) while it disfavors that of **Cu-I** that takes place at the triplet state (red-shifted).

Therefore, **Cu-X** (X = Cl or Br) and **Cu-I** are completely different luminophores despite their similar structures, and the fact that **Cu-Br** and **Cu-I** feature very similar emission quantum yield and lifetime at room temperature (table 2 and figure 4) is likely coincidental.

Excited State Pathways and Kinetics

The luminescence decays of the three complexes were recorded by time-correlated single photon counting (TC-SPC) in diluted dichloromethane solutions (figure 6a). The decays are biexponential, with a fast sub-nanosecond phase and a longer one (tens of nanoseconds).

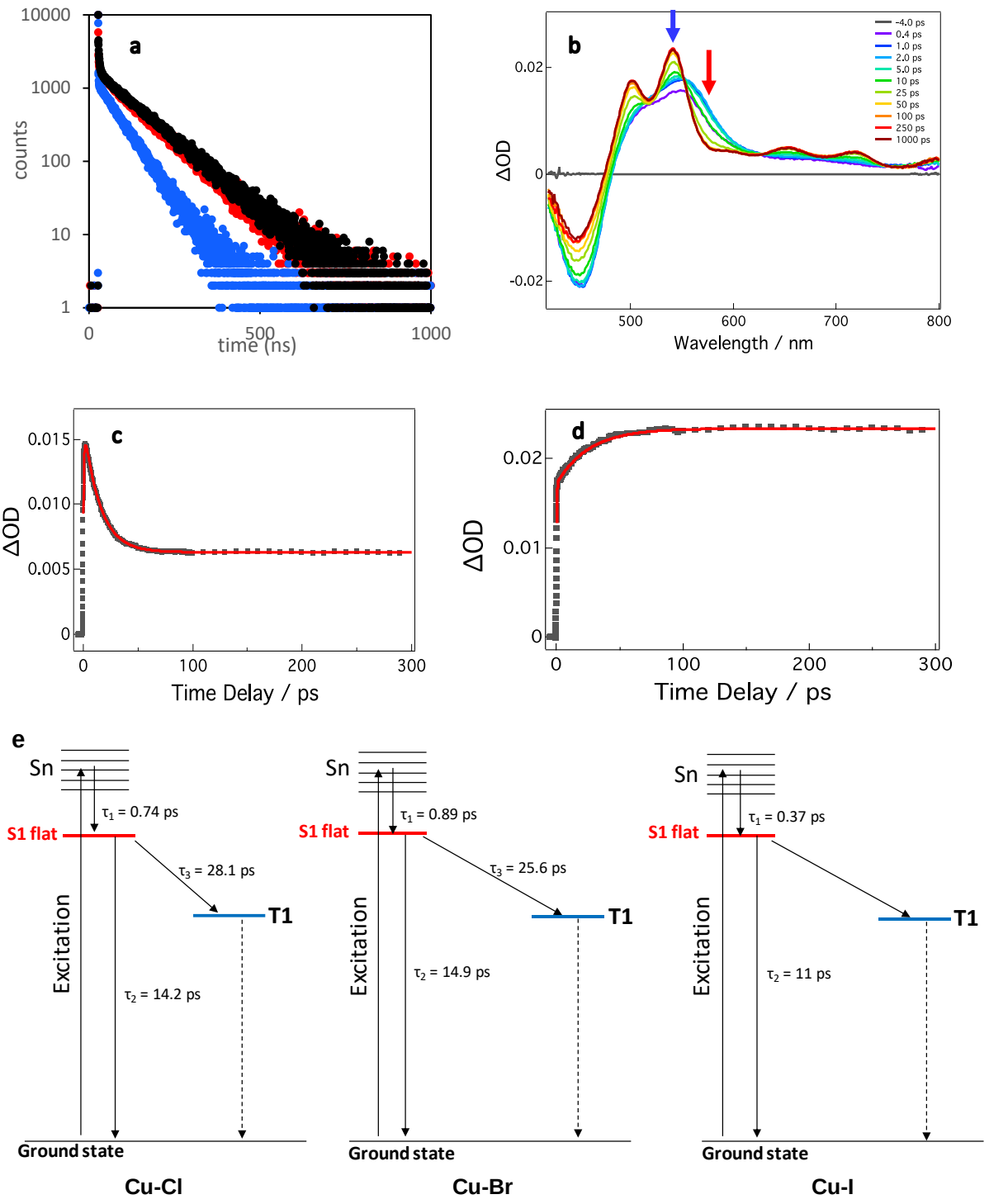

Figure 6. (a) luminescence decay in degassed dichloromethane for the **Cu-X** compounds (**Cu-Cl** in blue, **Cu-Br** in red and **Cu-I** in black). (b) Transient spectra for **Cu-Br** in degassed dichloromethane solution obtained after excitation at 415 nm. The red and blue arrows indicate the wavelengths where the kinetics of the singlet and triplet states were probed, respectively. (c) and (d): kinetic traces (grey) extracted from transient absorption spectra of **Cu-Br** in dichloromethane at 580 nm (c) and 540 nm (d). Red: best fit of the experimental data. (e) Simplified Perrin-Jablonski diagram for **Cu-X**.

The former can be associated to emission from non-relaxed hot states. The intersystem crossing being a very fast process[21,40] (less than 20 ps, see below), phosphorescence from multiple triplet MLCT states decay pathways is likely. In this particular case, two possible pathways could participate to the short-lived luminescence component, one from a triplet state where the complex does not (or feebly) interact with the solvent, another from a triplet state where the complex does interact with the solvent molecules. The longer-lived signals (63 ns for **Cu-Cl**, 106 ns for **Cu-Br**, and 110 ns for **Cu-I**, measured at maximum emission wavelengths for all complexes) are assigned to a radiative process involving the triplet state.[41] This is confirmed by the obvious quenching of the luminescence in presence of O_2 (figure S7).

Ultrafast transient absorption spectroscopy allowed to identify the various photo-induced processes at stake within the three complexes. Femtosecond transient absorption (TA) measurements (excitation at 415 nm) were performed on degassed dichloromethane solutions of **Cu-Cl**, **Cu-Br** and **Cu-I**. The TA spectrum of **Cu-Br** is given in figure 6b, **Cu-Cl**'s and **Cu-I**'s are presented in supporting information (figures S8 and S9). All complexes behave rather similarly, showing the usual behavior of copper(I)-bis(phenanthroline) complexes,[21,42] epitomized by benchmark $[Cu(dmp)_2]^+$.[43] After excitation, the transient spectra are dominated by a negative signal around 450 nm, assigned to the ground state bleach, and a broad featureless signal spanning between 500 and 600 nm. The latter is the spectral signature of the excited charge separated state where an electron has shifted from the copper ion to one of the two coordinated phenanthroline ligands. This signal then blue shifts and narrows (ca. 10 picoseconds timescale) into a camel back-shaped absorption bands manifold for **Cu-Cl** and **Cu-Br**. Again, **Cu-I** shows a peculiar behavior: its transient spectra are significantly less resolved, but humps are clearly visible as well a few picoseconds after excitation. Those were previously assigned to triplet excited state absorption features concomitant with vibrational cooling (relaxation of the coordination sphere).[43,44] The difference in the TA spectral features clearly suggests the electronic effect of the halogen groups at the 2,9-position on the energetics of the ligand anion state.

The transient kinetics of the singlet state S_1 were probed for all complexes on the red part of the transient absorption features (570-580 nm, figure 6c and figures S10 and S11) where the triplet absorption is the weakest, allowing to estimate the timescales for the spectral evolution of the excited state absorption band. All simulated data are gathered in table 3, and reported in the simplified Perrin-Jablonski diagram (figure 6e). For all complexes, the traces consist in a sub-picosecond rise (τ_1) shortly followed by a decay on a longer timescale (τ_2). τ_1 has been assigned to the lifetime for the formation of the lowest singlet state S_1 from the higher lying states manifold, while τ_2 has been attributed to S_1's decay.

The transient kinetics of the triplet state T_1 were monitored in the case of **Cu-Cl** and **Cu-Br**, following the evolution of the triplet transient absorption maxima (530 nm for **Cu-Cl**, 540 nm for **Cu-Br**). Both complexes exhibit a double exponential behavior with a sub-picosecond component associated to the singlet formation (because singlet and triplet absorptions significantly overlap) and a longer phase (whose lifetime is noted τ_3) assigned to the intersystem crossing (ISC), namely the triplet population from the singlet state. As commonly observed in copper complexes, ISC is thus taking place on a ca. 20 ps time scale.

In the case of **Cu-I**, the less structured transient spectra prevented us from distinguishing the triplet state formation from S_1, and the (very long lived, > 10000 ps) triplet state decay. This prevents us from comparing ISC kinetics among all complexes. However, one notices that all transient processes associated to the singlet state (τ_1 and τ_2) are significantly faster for **Cu-I** compared to **Cu-Cl** and **Cu-Br**. This has been previously observed by Castellano et al. in a series of complexes where the progressively increasing steric bulk was associated to shorter τ_1 and τ_2 time constants.[44] In other words, those short time constants in the case of Cu-I are in line with a more rigid environment around copper(I).

	τ_1 (ps)	τ_2 (ps)	τ_3 (ps)
Cu-Cl	0.74 ± 0.02	14.2 ± 0.2	28.1 ± 0.3
Cu-Br	0.89 ± 0.03	14.9 ± 0.1	25.6 ± 0.1
Cu-I	0.37 ± 0.04	11.0 ± 0.2	> 10000

Table 3. Lifetimes of the various photo-induced processes, extracted from simulated kinetic traces recorded after excitation at 415 nm.

Interestingly, the singlet decay (τ_2) is faster than the triplet population (τ_3), showing that another fast process depleting the singlet state is taking place in parallel to ISC. The nature of this process is unknown at the moment and its study is beyond the scope of the present work. However, the presence of isobestic points at 552 nm and 628 nm indicates direct conversion of one state to another (figure S12).

Theoretical Analysis.

Structures and absorption spectra. Upon geometry optimization the structures of the **Cu-X** series of complexes converged towards D_{2d} minima. The main geometrical parameters are reported in Table 4. The theoretical Cu-N distances agree well with the experimental results (Table 1) though the global shape is different from the one observed in the crystal. In the optimized structure in solution the two phenanthroline ligands are orthogonal whereas they are bent in the crystal. This difference arises from the intermolecular interactions in the solid phase between assembled complexes. The structure is very similar for the three **Cu-X** complexes. There are no differences concerning the copper-phenanthroline core.

	Cu-N	Cu-X	C-C	C-X	C-C-C	C-C-X
Cu-Cl	2.023	3.407	1.431	1.745	117.4	116.8
Cu-Br	2.011	3.476	1.432	1.918	117.5	116.6
Cu-I	2.044	3.585	1.431	2.126	117.6	116.5

Table 4. Bond lengths and angles of interest in the optimized structures of **Cu-X** complexes (X= Cl, Br and I). Calculated structures (in the ground state) are given in figure S13.

The frontier orbitals are also very similar among the complexes (see figure S4). The HOMO-2 of each complexes is an almost pure 3d orbital of the copper, the HOMO-1 and HOMO being σ^*_{Cu-N} orbitals. The four lowest unoccupied orbitals (LUMO to LUMO+3) are π^* orbitals localized on the phenanthroline moieties with small or no contribution of the halide. The absorption spectra depicted in Figure 7 were computed on the optimized structures of each complex.

The calculated absorption spectra of the three **Cu-X** complexes present similar features with a weak absorption in the visible spectral region (**Cu-Cl**: 471 nm, **Cu-Br**: 484 nm and **Cu-I**: 491 nm). A number of low-lying singlet states present at lower energy do not absorb. A weaker band appears at 424 nm (**Cu-Cl**), 432 nm (**Cu-Br**) and 438 nm (**Cu-I**). All these states correspond to metal-to-ligand charge transfer (MLCT) transitions corresponding to excitations from HOMO and/or HOMO-1 towards LUMO to LUMO+3 orbitals. A number of MLCT transitions from deeper orbitals of the copper are also present below 400 nm without absorbing intensities. The upper part of the absorption spectra (350-250 nm) is characterized by intense bands attributed to purely ligands localized transitions. These transitions present mixed ligand-centered (LC) / ligand-to-ligand charge transfer (LLCT) character (Figure 8).

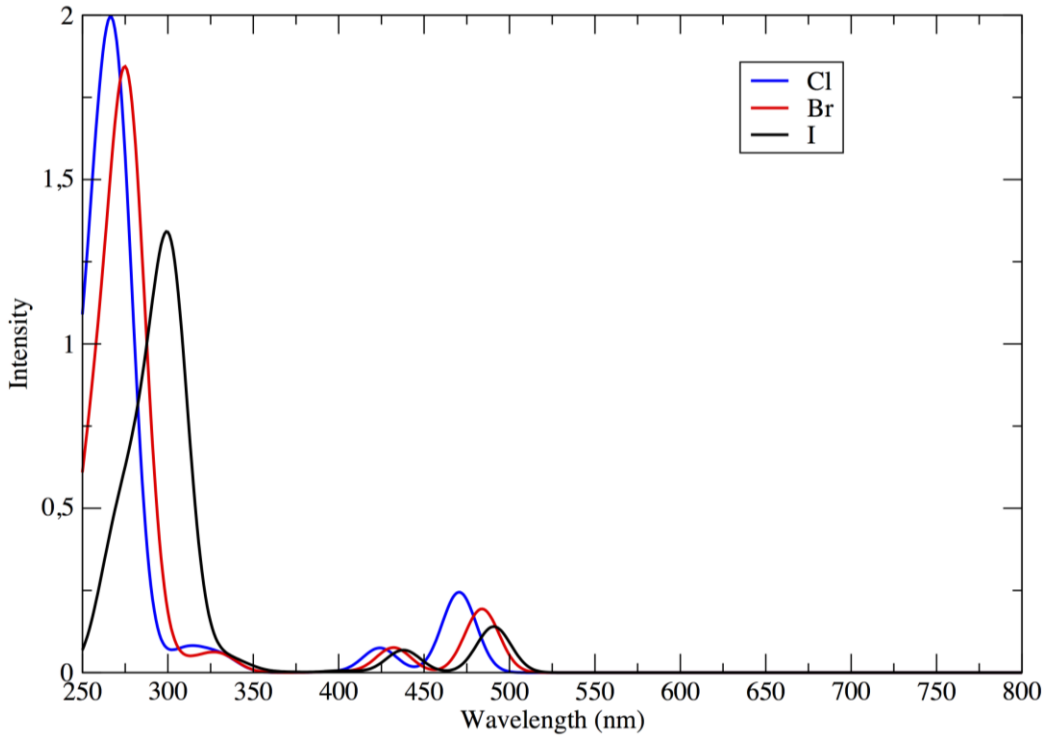

Figure 7: TD-DFT computed absorption spectra of the **Cu-X** complexes in DCM.

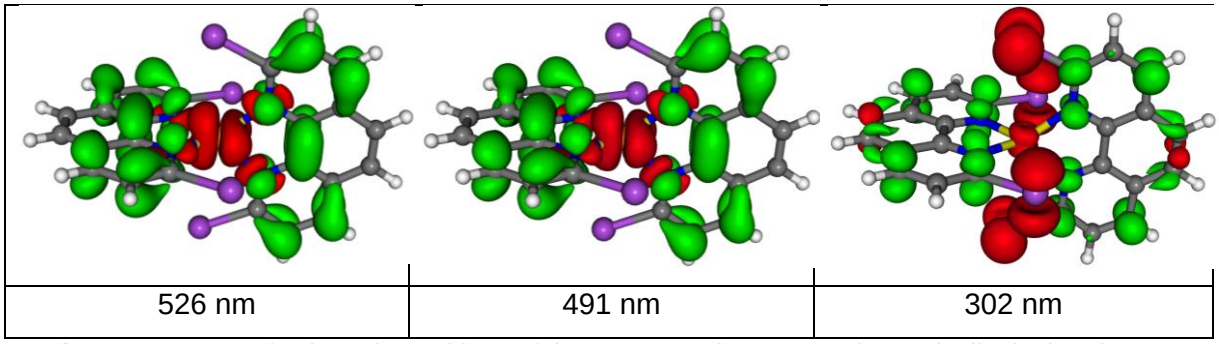

Figure 8: Nature of selected transitions of the **Cu-I** complex. Areas electronically depleted upon transition are displayed in red and areas electronically enriched in green (the MLCT states at 526 and 491 nm differ by the nature of the depopulated d_{Cu} orbital).

The absorption spectra computed on the optimized structure of each complex reproduce the experimental features in terms of position, intensities and redshift of the bands within the series **Cu-Cl**, **Cu-Br** and **Cu-I**. Spin-Orbit coupling effects are relatively small and do not modify drastically the shape of the absorption spectra. In order to take into account the nuclear flexibility of this class of molecules on the absorption spectrum, *Ab Initio* Molecular Dynamics (AIMD) simulations were performed on the three **Cu-X** complexes. The absorption spectra are then recomputed for a set of electronic ground state structures extracted from the AIMD trajectories. The generated absorption spectra including the dynamical effects are in excellent agreement with the experimental one (Figure 9).

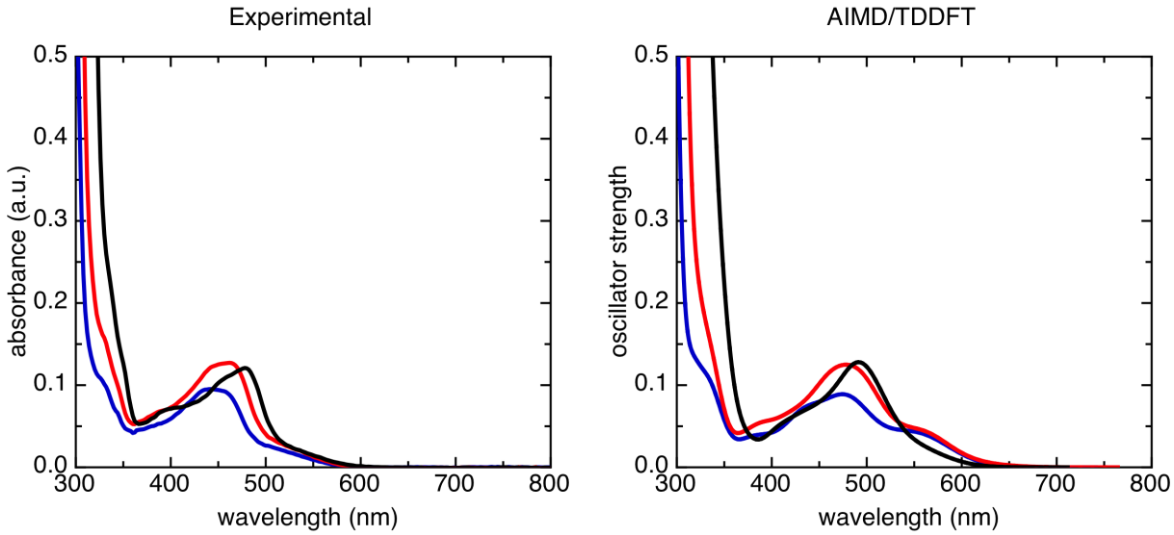

Figure 9: Compared experimental and theoretical (extracted from the AIMD) spectra for complexes **Cu-Cl** (blue), **Cu-Br** (red) and **Cu-I** (black).

The experimental absorption spectra have a tail beyond 500 nm which is assigned to the MLCT transitions that are dark in the D_{2d} structure. These states gain some oscillator strength in the D_2 structure, i.e. after flattening (Figure 8, state at 526 nm). The dynamical effects include the distortion of the phenanthroline ligands giving to these MLCT transitions some intensity.[45] This is well documented in a number of strongly distorted copper(I) complexes such as $Cu(dpp)_2^+$ or $Cu(dap)_2^+$ (where dap is 2,9-dianisyl-1,10-phenanthroline and dpp is 2,9-diphenyl-1,10-phenanthroline).[13,46] Interestingly, the transition is more pronounced for **Cu-Cl** and **Cu-Br** than **Cu-I** (as experimentally observed, see figure S14), as a consequence of a less distorted structure for the latter complex. Similarly, the originally dark MLCT transitions present between 350 and 400 nm (around 10) acquire some oscillator strength and are responsible for the absorbance in this domain.

Emission. Three sets of calculations were performed in order to understand the luminescence properties of the Cu(I) complexes. Indeed, the complexes belong to the D_{2d} symmetry group in their ground state. However, upon excitation symmetry is partially broken because of the well-established ligand flattening in this class of molecules[41,42,43,47] leading to the lower D_2 symmetry in which the two phenanthroline remain identical. Further C_2 symmetry reduction leads to Cu-N distances lengthening in one phenanthroline and to Cu-N distances shortening in the other one (figure 10). The singlet and triplet excited state minima were obtained under this C_2 symmetry constraint. In addition, the lowest excited singlet and triplet excited state potential energy surfaces exhibit highly distorted structures of C_1 symmetry. It is worth noting that the structures of the excited singlet and triplet states are similar for a given symmetry group and that structural evolution is nearly similar for the three complexes.

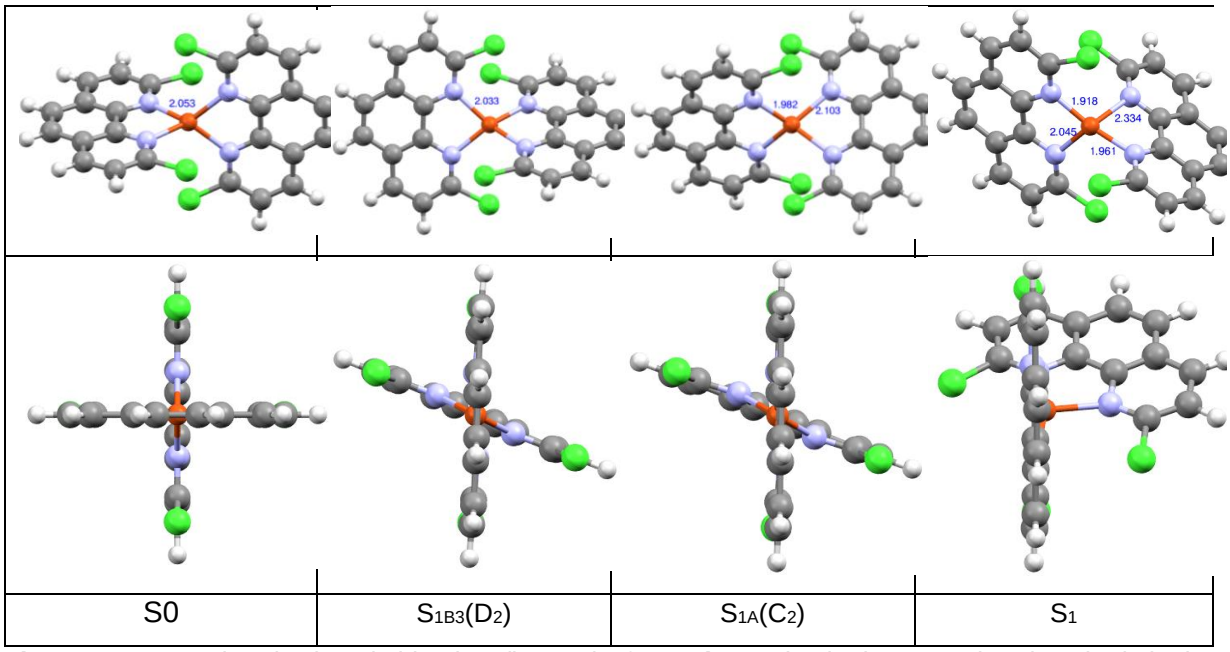

Figure 10. Front view (top) and side view (bottom) of **Cu-Cl** complex in the ground and excited singlet states. In blue are the Cu-N distances in Å.

We computed the excited singlet and triplet states in each symmetry group (see SI for all calculated structures). Three S_1/T_1 sets of optimized structures were obtained: the first one under D_2 symmetry constraint, S_{1B3}/T_{1A}, the second one under C_2 symmetry constraint, S_{1A}/T_{1A}, and the third one S_1/T_1 without any symmetry (C_1). The lowest D_2, C_2 and C_1 optimized singlet and triplet states (Table 5) origin from the MLCT states described in Figure 8. Whereas these states are delocalized on both phenanthroline in D_2 structures, they localize on one ligand in reduced C_2 symmetry as illustrated by the electronic densities differences depicted in figure 11.

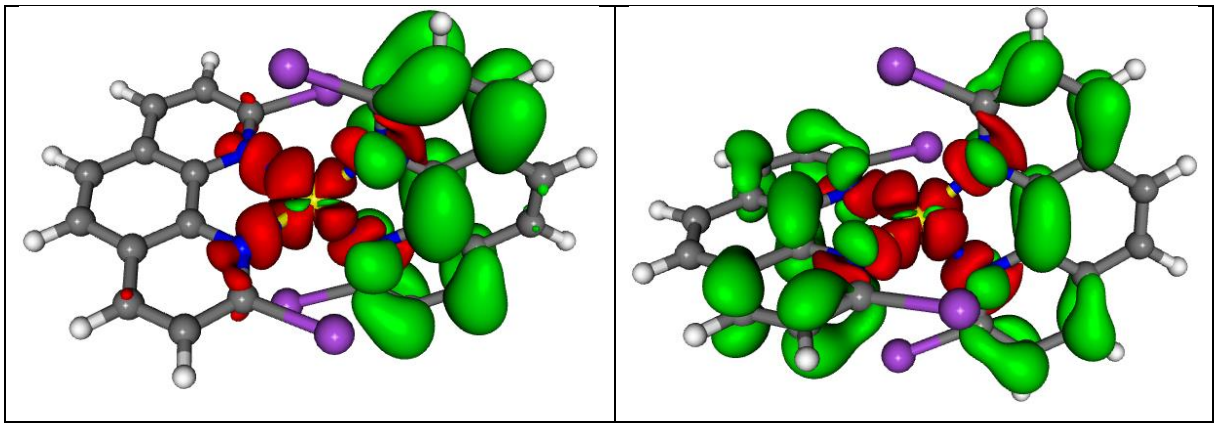

Figure 11. Nature of $S_{1A}(C_2)$ (left) and $S_{1B3}(D_2)$ (right) of the **Cu-I** complex. In red areas electronically depleted upon transition and in green areas enriched.

This generates two degenerate singlet and triplet states. We also evidenced the presence of highly distorted structures when totally relaxing the symmetry (C_1 point group). In these geometries, three N atoms form a triangle in which the copper occupies the center. The three

complexes behave similarly with one noticeable exception. Indeed, for the **Cu-I** complex no flattening is observed for the lowest excited singlet of C_2 symmetry (figure 12) whereas flattening is observed for all other structures whatever the complex or state considered. This could be due to the larger size of iodine *vs.* bromine and chlorine. Moreover, the bigger steric strain imposed by I is in line with a high emission quantum yield (and favored ISC[48] as confirmed by the larger rate constants monitored by transient absorption spectroscopy). Very importantly, this explains the drop in the oscillator strength by two orders of magnitude for the $S_{1A}(C_2)$ state of the **Cu-I** complex ($f \approx 10^{-5}$) as compared to the values obtained for the **Cu-Br** and **Cu-Cl** complexes ($f \approx 10^{-3}$).

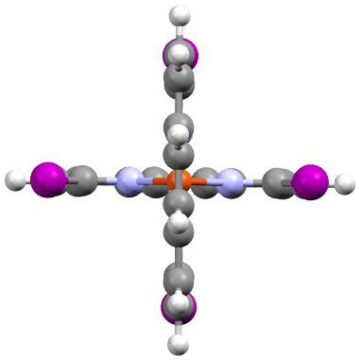

Figure 12. Side view of the $S_{1A}(C_2)$ optimized structure of the **Cu-I** complex showing the absence of flattening.

Upon geometry relaxation, the excited states are significantly stabilized as illustrated by the calculated emission wavelengths reported in Table 5 for the three complexes.

	Exp	$S_{1B3}(D_2)$	$T_{1A}(D_2)$	$S_{1A}(C_2)$	$T_{1A}(C_2)$	S_1 (C_1)	T_1 (C_1)
Cu-Cl	715	681 ($6.5\ 10^{-2}$)	902	845 ($8.0\ 10^{-3}$)	975	812 ($2.9\ 10^{-3}$)	934
Cu-Br	700	673 ($5.8\ 10^{-2}$)	856	805 ($8.9\ 10^{-3}$)	927	824 ($2.0\ 10^{-3}$)	905
Cu-I	700	652 ($4.3\ 10^{-2}$)	779	710 ($6.3\ 10^{-5}$)	862	864 ($1.7\ 10^{-3}$)	937

Table 5: Compared experimental and theoretical emission wavelengths (in nm) of the lowest singlet and triplet states under D_2, C_2 and C_1 symmetry constraints and associated oscillator strengths (between brackets) for the singlet states.

Within the limit of the present static picture, the computed emission wavelengths when relaxing totally the structures (C_1) differ significantly from the experimental data (table 5) for the three complexes, either in the singlet or in the triplet states. It is worth noting that the calculated

singlet emission wavelengths under D_2 or C_2 symmetry constraints are in good agreement with the experimental data. A further qualitative interpretation of the luminescent properties and TADF is based on the energetics of the lowest singlet and triplet potential energy surfaces discussed below.

The analysis of the distortion and emission energies, E_{dist} and E_{em}, respectively, together with the relative position of the excited state potential wells minima (E_{min}) reported in Table 6 evidences the absence of a significant energy barrier between the two degenerate C_2 structures. This offers the possibility to the systems at room temperature to easily relax from one C_2 potential well to the other one *via* the D_2 structure.

Cu-Cl	$S_{1B3}(D_2)$	$T_{1A}(D_2)$	$S_{1A}(C_2)$	$T_{1A}(C_2)$	S_1	T_1
E_{dist}	0.410	0.568	0.697	0.633	0.697	0.643
E_{em}	1.821	1.375	1.467	1.272	1.527	1.328
E_{min}	2.231	1.943	2.164	1.905	2.224	1.973
ΔE_{S-T}	0.287	0.361	0.198	0.339	0.130	0.265
SOC	20	17	37	56	14	43

Cu-Br	$S_{1B3}(D_2)$	$T_{1A}(D_2)$	$S_{1A}(C_2)$	$T_{1A}(C_2)$	S_1	T_1
E_{dist}	0.401	0.534	0.637	0.598	0.776	0.741
E_{em}	1.842	1.448	1.540	1.337	1.504	1.371
E_{min}	2.243	1.982	2.177	1.935	2.281	2.111
ΔE_{S-T}	0.260	0.333	0.198	0.319	0.117	0.165
SOC	23	21	39	57	13	24

Cu-I	$S_{1B3}(D_2)$	$T_{1A}(D_2)$	$S_{1A}(C_2)$	$T_{1A}(C_2)$	S_1	T_1
E_{dist}	0.391	0.464	0.442	0.564	0.874	0.814
E_{em}	1.900	1.592	1.747	1.438	1.435	1.324
E_{min}	2.291	2.056	2.189	2.002	2.309	2.137
ΔE_{S-T}	0.195	0.266	0.154	0.255	0.115	0.151
SOC	24	22	4	52	12	21

Table 6. Distortion energy of the ground state in the geometry of the excited state (E_{dist} in eV), emission energy of the excited state (E_{em} in eV) and energy of the minima of the excited states (E_{min} in eV). Singlet-triplet splitting in eV (ΔE_{S-T}) (for the considered state in the considered geometry) and

norm of the Spin-Orbit Coupling (SOC) in cm^{-1}. Only the values for the lowest singlet and triplet state is given for each symmetry, see SI for the other states (tables S2 to S7).

Indeed, the energy differences between $S_{1B3}(D_2)$ and $S_{1A}(C_2)$ or $T_{1A}(D_2)$ and $T_{1A}(C_2)$, which give an estimation of the energy barrier between the minima corresponding to the electronic localization on one or the other phenanthroline (Figure 11), never exceeds 0.1 eV.

This small energy barrier can easily be overcome at room temperature,[49] either on the singlet or on the triplet potential energy surface opening deactivation channels that will affect the TADF efficiency and the luminescent properties. This is illustrated by the energy profiles represented in Scheme 1 for the lowest triplet and singlet states that connect the three structures, from the delocalized one over the two phenanthroline (D_2) to the totally relaxed (C_1) *via* the localization on one phenanthroline (C_2). The mirror profiles corresponding to the delocalization on the other phenanthroline are not represented here for the sake of clarity.

TADF processes. Starting from the D_2 structures at room temperature we may propose the following qualitative mechanisms (Scheme 1):

The **Cu-Cl** complex is characterized by a larger ΔE_{S-T} and a smaller SOC at T_1 geometry $T_{1A}(D_2)$ than at S_1 geometry $S_{1B3}(D_2)$ (Table 6). This makes the r-ISC less efficient with a larger contribution of the triplet state to the emission not in favor of a TADF mechanism. This generates a broad signal of low intensity. In addition the low energy triplet C_1 structure calculated at 0.068 eV above the triplet C_2 structure T_{1A} (C_2) is easily accessible disfavoring any back population of the singlet potential energy surface as well as fluorescence. When decreasing the temperature this effect is accentuated trapping the system into the low-lying triplet potential wells and thus opening the way to non-radiative decay, which materializes in the largest k_{nr} in the series (table 2).

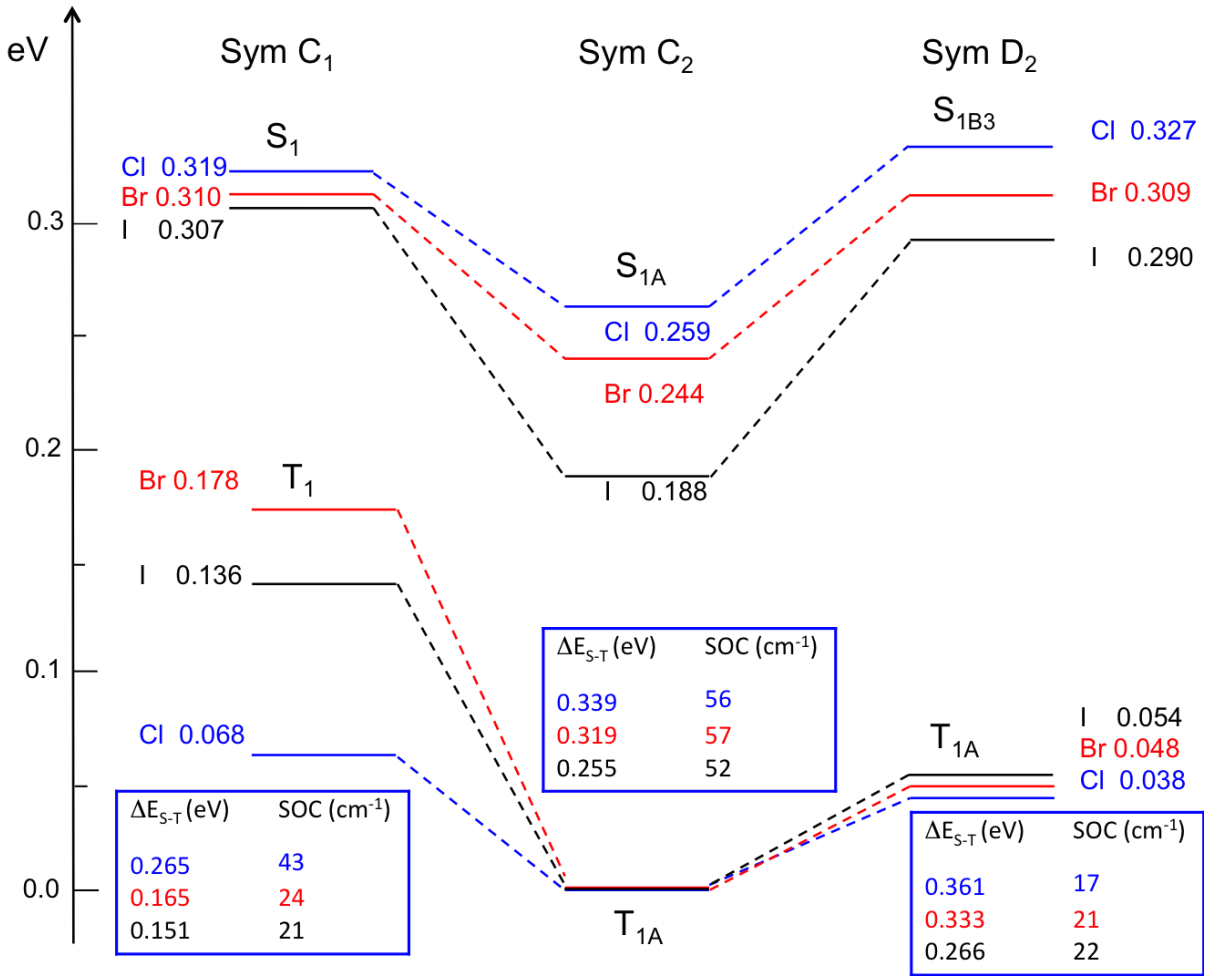

Scheme 1. Potential energy profiles (in eV) of the lowest singlet and triplet excited states of **Cu-Cl** (in blue), **Cu-Br** (in red) and **Cu-I** (in black) complexes, ΔE_{S-T} (in eV) and SOC (in cm^{-1}) at the triplet structures and relative energies (in eV) to the lowest triplet T_{1A} (C_2) taken as reference.

In the **Cu-Br** complex, the ΔE_{S-T} behaves similarly but the SOC at T_1 geometry is stronger than at S_1, making the r-ISC process more efficient and enhancing the emission from the singlet state compatible with a TADF mechanism. Relaxation to the C_2 structures along the singlet potential is responsible for the long tail of the luminescent signal observed beyond 750 nm. Lowering the temperature should enhance this effect and consequently weaken the TADF process. In contrast to **Cu-Cl** this complex should not fully relax to the C_1 triplet structure calculated at 0.178 eV above the C_2 triplet structure preventing any dramatic loss of luminescence.

The **Cu-I** complex differs from the previous molecules by several features. At the D_2 structures a TADF mechanism is theoretically active because of a small ΔE_{S-T} and a significant SOC with a luminescence at 652 nm, slightly blue-shifted with respect to the experimental maximum (700 nm). However, efficient relaxation to the C_2 structures, accentuated at low temperature, will trap the system in the S_{1A} (C_2) potential well, especially deep for the **Cu-I** system. At this

structure and despite of the large SOC (52 cm^{-1}) and small ΔE_{S-T} (0.255 eV) the singlet is weakly emissive with a calculated oscillator strength of about 10^{-5}. Moreover, the small energy gap between the T_1 (C_1) and S_{1A}(C_2) minima (< 0.06 eV) makes the relaxation *via* a spin-vibronic mechanism[40] to the C_1 structure highly probable. Walking on the triplet potential energy surface the molecule may either emit from the S_1 (C_1) structure at 864 nm after r-ISC from T_1 (C_1) or emit from both the T_{1A} (C_2) and T_{1A} (D_2) at 862nm and 779 nm, respectively, at the expense of the TADF activity as monitored by the temperature dependent steady state emission study.

The above detailed analysis illustrates the difficulty at using basic concepts such as energy gap law valid only in simple cases of nested S_1 and T_1 potentials.[50] Further study of the emissive properties of this class of complexes should include nuclear relaxation effects by means of MD simulations. Moreover, vibronic coupling effects may contribute to the TADF mechanism in addition to the SOC effects as shown recently for dinuclear Cu(I) complexes.[51] Further modeling of the emissive properties of this class of complexes should include dynamical effects[52] which are beyond the scope of the present study.

Conclusion

The synthesis and full physical characterization of three new photosensitive copper(I) complexes **Cu-X** ($Cu(\mathbf{L_X})_2^+$ where $\mathbf{L_X}$ is a phenanthroline ligand substituted in α of the chelating nitrogen atoms by halogen atoms) are reported. All complexes are luminescent and display the usual transient absorption features of copper(I)-bis(phenanthroline) complexes. Nevertheless, transient signals for the couple **Cu-Cl** and **Cu-Br** are similar while **Cu-I** differentiates itself with shorter singlet S_1 rise and decay, in favor of a more rigid environment for the latter. The trend in emission quantum yield Φ and lifetime τ is consistent with the increasing size of the halogen substituents, in line with common knowledge that the larger the bulky groups in positions 2 and 9 of phenanthroline, the larger Φ and τ. However, we monitored a more intense luminescence for **Cu-Br** and **Cu-I** than for benchmark $Cu(dmp)_2^+$, showing that the excited state properties of copper(I) complexes are not necessarily related only to steric strain.

Moreover, while **Cu-Cl** and **Cu-Br** display the usual thermally activated delayed fluorescence mechanism, **Cu-I** exhibits the opposite behavior (i.e. Φ increases when T decreases) revealing that the overall emission stemming from the lower lying triplet state is favored *vs.* singlet emission in this case. Importantly, this last feature makes **Cu-I** a much better luminophore than **Cu-Cl** and **Cu-Br** especially at low temperature. Theoretical calculations provide a rationale for this unexpected (and to the best of our knowledge never experienced before) behavior. To

summarize, quantum mechanics calculations performed in three different symmetries (in order to take into account the very significant reorganization of the copper(I)-bis(diimine) coordination sphere in the excited state) revealed that a TADF mechanism is in principle possible for **Cu-I**. Indeed, a smaller $\Delta E_{S\text{-}T}$ and a high SOC in the triplet state tend to favor rISC (as observed for **Cu-Cl** and **Cu-Br**). However, in the particular case of **Cu-I**, emission from the more stable singlet state (in C_2 symmetry) is endowed with a very weak oscillator strength. This latter fact is due to stronger rigidity of the coordination scaffold. Thus, populating the singlet state(s) by thermal rISC is detrimental to the overall luminescence of the complex. The experimental observation that the triplet state be endowed with a higher luminescence quantum efficiency in the case of **Cu-I** has not been fully rationalized yet. However, let us pinpoint that the excited state for all three complexes tend to relax in the C_2 symmetry (showing the deeper energy wells, scheme 1) but the well is a lot deeper (S_{1A}) for **Cu-I** than **Cu-Cl** and **Cu-Br** (where they are similar). Thus, while multiple internal conversion and intersystem crossing processes from S_{1A} are possible for **Cu-Cl** and **Cu-Br** (consequently increasing the probability of non-radiative processes) **Cu-I** gets trapped more efficiently in S_{1A}, limiting non radiative pathways, a feature accentuated at low temperature.

Associated Content

Evolution of the absorbance of complexes **Cu-X** in dichloromethane upon addition of aliquots of acetonitrile, evolution of the MLCT upon addition of CH_3CN into CH_2Cl_2 solutions of **Cu-X**, cyclic voltammograms for **Cu-X**, HOMO and LUMO, absorption spectra of the electrolytic medium after electrolysis of a **Cu-Br** solution, evolution of the steady state emission spectra for **Cu-X** complexes with the temperature in dichloromethane, luminescence decays for **Cu-X** complexes in aerated and argon purged dichloromethane solutions, transient fs absorption spectra of **Cu-Cl** and **Cu-Br**, decay traces of the absorption profiles at given wavelengths for **Cu-Cl** and **Cu-I**, focus on the isobestic points at 552 and 628 nm for **Cu-I** transient absorption spectrum, selected views for computed structures of **Cu-Cl**, **Cu-Br** and **Cu-I** in their ground state S_0, normalized experimental absorption spectra of **Cu-X** complexes, with respect to absorbance and wavelength, absorption spectra computed for **Cu-X** (X = Cl, Br, I) considering from 20 to 120 snapshots from the AIMD simulations, energy (in eV) of the HOMO and LUMO orbitals of the **Cu-X** complexes in their ground state, distortion energy of the ground state in the geometry of the excited state (Edist in eV), emission energy of the excited state (Eem in eV), energy of the minima of the excited states (Emin in eV) and oscillator strength for D_2, C_2 and C_1 structures of the **Cu-X** complexes and main structural parameters of **Cu-X** average of selected structures and full dynamics can be found in the supplementary files.

Acknowledgments

The authors wish to thank the ANR (PERCO program n°ANR-16-CE07-0012-01) for financial support, the PIAM (Angers University, France) and the CEISAM (Nantes University) analysis platforms, the HPC of Strasbourg and IDRIS (project A0050810629) for computing facilities and the CNRS for funding. SBX was supported by funding from the National Science Foundation (CHE-1363007 to LXC). LXC is partially supported by Solar Energy and Photochemistry Program in CBGS Division, the U. S. Department of Energy, Office of Science, Office of Basic Energy Sciences, under Contract No. DE-AC02-06CH11357.

Experimental part

General: chemicals were purchased from Sigma-Aldrich or Fisher Scientific and used as received. Thin-layer chromatography (TLC) was performed on aluminium sheets precoated with Merck 5735 Kieselgel 60F254. Column chromatography was carried out with Merck 5735 Kieselgel 60F (0.040-0.063 mm mesh). ^{1}H NMR spectra were recorded on an AVANCE 300 UltraShield BRUKER. Chemical shifts for ^{1}H NMR spectra are referenced relative to residual protium in the deuterated solvent ($CDCl_3$ δ = 7.26 ppm). NMR spectra were recorded at room temperature, chemical shifts are written in ppm and coupling constants in Hz. Mass spectrometry was performed with a JEOL JMS-700 B/E spectrometer. Electrochemical measurements were made under an argon atmosphere in CH_2Cl_2 with 0.1 M Bu_4NPF_6. Cyclic voltammetry experiments were performed by using an Autolab PGSTAT 302N potentiostat/galvanostat. A standard three-electrode electrochemical cell was used. Potentials were referenced to a saturated calomel electrode (SCE) as internal reference. All potentials are quoted relative to SCE. The working electrode was a glassy carbon disk and the auxiliary electrode was a Pt wire. In all the experiments the scan rate was 100 $mV.s^{-1}$. UV-visible absorption spectra were recorded on a UV-2401PC Shimadzu, using 1 cm path length cells. Emission spectra were recorded on a Fluoromax-4 Horiba spectrofluorimeter (1 cm quartz cells). Luminescence decays were recorded with a DELTAFLEX time correlated single photon counting system (HORIBA) on degassed dichloromethane solutions.

Temperature dependent fluorescence spectroscopy: for every sample, measurements were performed on freeze-pump-thaw degassed dichloromethane solution of the sample cannulated inside an argon-purged capillary quartz tube. The quartz tube was sealed with Teflon cork and parafilm, then set into an Oxford Instrument cryostat (Optistat CF2) insert directly in the sample chamber of the spectrofluorimeter. Luminescence spectra were

measured using a Horiba-Jobin-Yvon Fluorolog-3® spectrofluorimeter, equipped with a three-slit double-grating excitation and emission monochromator with dispersions of 2.1 nm.mm-1 (1200 grooves.mm-1), and a R928 detector operating in the visible. Measurements were performed every 10 K, in the range 333-183K. Spectra were reference corrected for both the excitation source light intensity variation (lamp and grating) and the emission spectral response (detector and grating). Excitation wavelength was 480nm, emission was collected in the 550-800 nm range. Because of the low emission intensity associated with Cu complexes (QY<0.01) excitation and emission slits were set at 5 nm each, to ensure sufficient signal detection for relevant comparison of the data.

Transient absorption: Femtosecond transient absorption measurements were performed using an amplified Ti:Sapphire laser system (Spectra Physics, Spitfire Pro) and an automated data acquisition system (Ultrafast Systems, Helios). The amplifier was seeded with the 100 fs output from the oscillator (Spectra Physics, Mai Tai) and was operated at 1.0 kHz, giving 3 mJ pulses centred at 830 nm. The beam was split 90/10, with the weaker beam being used to generate the white light continuum probe. The probe beam was delayed relative to the pump with a retroreflector mounted on a motorized delay stage and focused into a sapphire plate to generate a white light continuum spanning 420 to 650 nm. The continuum probe was focused to a spot size of 200 μm at the sample and subsequently focused into a fibre optic coupled to a multichannel spectrometer and CMOS sensor. The other 830 nm beam was focused into a BBO crystal to generate the 415 nm pump beam used for the pump–probe measurements. This beam was passed through a depolarizer, chopped at 500 Hz, focused at the sample position to a spot size of 400 μm, and attenuated to a pulse energy of 2 μJ. Transient absorption spectra were collected using the Helios control software. The data were corrected for temporal chirp in the probe beam using the separately collected nonresonant response of the blank solvent. The nonresonant response gave an instrument response time of approximately 300 fs. All experiments were performed at room temperature with constant stirring with samples in 2 mm quartz cuvettes that had been bubbled with nitrogen.

X-ray crystallography: A crystal of "2,9-di-chloro-1,10-phenanthroline" was mounted on MicroLoops. The intensity measurement was carried out at 293 K on a Bruker-Nonius Kappa CCD diffractometer, using graphite-monochromatized Mo*K*-$L_{2,3}$ radiation (λ = 0.71073 Å) up to a resolution of $(\sin\theta/\lambda)_{max}$ = 0.66 $Å^{-1}$. The structure was solved using the charge flipping algorithm[53] implemented in the Superflip program[54] and refined with JANA2006 program[55] against F^2 for all reflections. Non-hydrogen atoms were refined with anisotropic displacement parameters. All H atoms were introduced in geometrically optimized positions and refined with a riding model. CCDC-1884336 contains the supplementary crystallographic data. These data

can be obtained free of charge from the Cambridge Crystallographic Data Centre via www.ccdc.cam.ac.uk/data_request/cif.

Crystal data C_{24} H_{12} N_4 Cl_4 Cu P F_6:, Mr = 706.7, monoclinic, P21/n, a =7.5379 (5), b = 23.884 (5), c = 14.676 (3) Å, V = 2620.0(8) Å3, Z =4, ρ_{calcd} = 1.7916 g.cm^{-3}, μ = 0.137 mm^{-1}, F(000) = 1400, plate, 0.51 × 0.32 × 0.06 mm^3, T = 293 K, 44490 reflections, 6154 unique (99% completeness), 361 parameters, GOF = 2.29, wR2 = 0.1998, R = 0.0735 for 4139 reflections with I > 2σ(*I*).

Computational Details: all static calculations were performed with ADF 2013 package (ADF, SCM, Theoretical Chemistry; Vrije Universiteit: Amsterdam, The Netherlands, 2013; Online at https://www.scm.com/ Downloads/) at DFT level of theory with B3LYP functionnal.[56] All atoms were described by the triple-ζ basis set.[57] Weak interactions were included through the Grimme3 corrections[58] and relativistic effects through ZORA hamiltonian.[59] Solvent corrections (namely dichloromethane) were included through a COSMO model.[60] Geometries of the electronic ground states of the three complexes were fully optimized and UV-Visible spectra computed on the subsequent structures by mean of TD-DFT including Tamm-Dancoff corrections.[61] Spin-Orbit Couplings (SOC) were computed perturbatively[62] from the TD-DFT results. Only the fast response of the solvent was included in the TD-DFT by setting the Neql parameter at 2.019. The structures of the electronic excited states were fully optimized at the same level of theory under various symmetry constraints and used for calculating distortion energies, emission energies and singlet-triplet energy gaps. To take into account the structural flexibility of the complex in the computation of the absorption spectra, *Ab Initio* Molecular Dynamics (AIMD) were performed. AIMD are done in gas phase within the Born-Oppenheimer formalism using the PBE density functional[63] with D2 correction of Grimme.[64] A kinetic energy cutoff of 35 Ry was selected for the description of the valence electrons with Vanderbilt ultrasoft pseudopotentials for the core electrons.[65] A Berendsen thermostat[66] has been employed at a temperature of 300 K using a time step of 25 Rydberg atomic units (1.2094 fs). The system is equilibrated for 1.2 ps and the dynamics run up to 8.5 ps giving a total of 7.3 ps of production time. The simulation is performed in a cubic cell of 60 Bohr^3 where the Makov-Payne correction[67] is applied to ensure that the molecule is isolated from their virtual counterparts in periodic boundary conditions. The spin-orbit free absorption spectra have been computed for 120 equidistant geometries extracted from the production time of the AIMD dynamics. The main structural parameters investigated were the Cu-N and the C-X distances, the N-Cu-N angle and the N-N-Cu-N dihedral angle. In order to evaluate the adequacy of the selection, the average of these parameters were compared between the selected structures and the full dynamics. The average values obtained are provided in table S8 as well as the definition of the parameters (figure S15). For each geometry 50 singlets are calculated by means of TD-

DFT at the same level described above. From the energies and oscillator strength at all geometries the spectra are computed as a sum of Gaussians. In order to smooth any artificial structure of the spectrum arising from the random sampling, a full-width at half-maximum (FWHM) of 0.2 eV is employed. AIMD simulations were done using Quantum Espresso package (version 5.1.1.).[68] The sampling dependence of the absorption spectra was investigated for the three complexes in order to ensure full convergence. In figure S16 are given the spectra computed considering from 20 to 120 structures extracted from the AIMD in each case. All computed structures are provided in the Cu-Cl.xyz, Cu-Br.xyz and Cu-I.xyz files.

Synthesis: 2,9-di-chloro-1,10-phenanthroline,[69] 2,9-di-bromo-1,10-phenanthroline[70] and 2,9-di-iodo-1,10-phenanthroline[30] ligands, $Cu(CH_3CN)_4PF_6$[71] and **Cu-Cl** complex[25] were synthesized following literature procedures.

Synthesis of **Cu-Br**: $\mathbf{L_{Br}}$ (56 mg, 0.17 mmol) was dissolved in dichloromethane (20 mL) and thoroughly degassed under argon in an ultrasonic bath. To this solution was added $Cu(CH_3CN)_4PF_6$ (30.9 mg, 0.083 mmol, 0.5 eqv.) in one go. The solution immediately turned red and was left to stir at room temperature for one hour, under argon. The solution was filtrated, the filtrate was evaporated under reduced pressure, and the resulting powder was collected and washed with diethyl ether, affording pure **Cu-Br**. Yield: 70 mg (95%). ^{1}H NMR (300 MHz, $CDCl_3$, 25°C): δ = 8.53 (4H, d, J = 8.7 Hz), 8.18 (4H, s), 8.07 (4H, d, J = 8.7 Hz). HRMS (FAB+) $[M]^+$ m/z: calculated for $C_{24}H_{12}N_4Br_4Cu^+$: 734.7086; found: 734.7070. Δ = 2.8 ppm.

Synthesis of **Cu-I**: the same protocol than above was used, with L_I (50 mg, 0.12 mmol) and $Cu(CH_3CN)_4PF_6$ (21 mg, 0.06 mmol, 0.5 eqv.). Yield: 57mg (89%). ^{1}H NMR (300 MHz, acetone D_6, 25°C): δ = 8.37 (8H, m), 8.17 (4H, m). HRMS (FAB+) $[M]^+$ m/z: calculated for $C_{24}H_{12}N_4I_4Cu^+$: 926.6537; found: 926.6540. Δ = 0.3 ppm.

References

(1) Ramamurthy, V.; Turro, N. J. Photochemistry: Introduction. *Chem. Rev.* **1993**, *93*, 585-586.
(2) Hagfeldt, A.; Grätzel, M. Molecular Photovoltaics. *Acc. Chem. Res.* **2000**, *33*, 269-277; Grätzel, M. Recent Advances in Sensitized Mesoscopic Solar Cells. *Acc. Chem. Res.* **2009**, *42*, 1788-1798; Robertson, N. Optimizing Dyes for Dye‐Sensitized Solar Cells. *Angew. Chem. Int. Ed.* **2006**, *45*, 2338-2345.
(3) Bozic-Weber, B.; Constable, E. C.; Housecroft, C. E. Light harvesting with Earth abundant d-block metals: Development of sensitizers in dye-sensitized solar cells (DSCs). *Coord. Chem. Rev.* **2013**, *257*, 3089-3106.
(4) Andreiadis, E. S.; Chavarot-Kerlidou, M.; Fontecave, M.; Artero, V. Artificial Photosynthesis: From Molecular Catalysts for Light-driven Water Splitting to Photoelectrochemical Cells. *Photochem. Photobiol.* **2011**, *87*, 946-964; Amouyal, E. Water splitting: from molecular to supramolecular photochemical systems. *Wiley Ser. Photosci. Photoeng.* **1997**, *2*, 263-307; Berardi, S.; Drouet, S.; Francas, L.; Gimbert-Surinach, C.; Guttentag, M.; Richmond, C.; Stoll, T.; Llobet, A. Molecular artificial photosynthesis. *Chem. Soc. Rev.* **2014**, *43*, 7501-7519.
(5) Galian, R. E.; Perez-Prieto, J. Catalytic processes activated by light. *Energy Environ. Sci.* **2010**, *3*, 1488-1498; Palmisano, G.; Augugliaro, V.; Pagliaro, M.; Palmisano, L. Photocatalysis: a promising route for 21st century organic chemistry. *Chem. Commun.* **2007**, 3425-3437; Oelgemöller, M. Solar Photochemical Synthesis: From the Beginnings of Organic Photochemistry to the Solar Manufacturing of Commodity Chemicals. *Chem. Rev.* **2016**, *116*, 9664-9682; Narayanam, J. M. R.; Stephenson, C. R. J. Visible light photoredox catalysis: applications in organic synthesis. *Chem. Soc. Rev.* **2011**, *40*, 102-113.
(6)Campagna, S.; Puntoriero, F.; Nastasi, F.; Bergamini, G.; Balzani, V. In *Photochemistry and Photophysics of Coordination Compounds I*; Balzani, V., Campagna, S., Eds. 2007; Vol. 280, p 117-214; Abbotto, A.; Manfredi, N. Electron-rich heteroaromatic conjugated polypyridine ruthenium sensitizers for dye-sensitized solar cells. *Dalton. Trans.* **2011**, *40*, 12421-12438.
(7) Blaskie, M. W.; McMillin, D. R. Photostudies of copper(I) systems. 6. Room-temperature emission and quenching studies of bis(2,9-dimethyl-1,10-phenanthroline)copper(I). *Inorg. Chem.* **1980**, *19*, 3519-3522.
(8) Armaroli, N. Photoactive mono- and polynuclear Cu()-phenanthrolines. A viable alternative to Ru()-polypyridines? *Chem. Soc. Rev.* **2001**, *30*, 113-124.
(9) Armaroli, N.; Accorsi, G.; Cardinali, F.; Listorti, A. Photochemistry and photophysics of coordination compounds: copper. *Top. Curr. Chem.* **2007**, *280*, 69-115.
(10) Scaltrito, D. V.; Thompson, D. W.; O'Callaghan, J. A.; Meyer, G. J. MLCT excited states of cuprous bis-phenanthroline coordination compounds. *Coord. Chem. Rev.* **2000**, *208*, 243-266.
(11) Kirchhoff, J. R.; Gamache, R. E.; Blaskie, M. W.; Del Paggio, A. A.; Lengel, R. K.; McMillin, D. R. Temperature dependence of luminescence from Cu(NN)2+ systems in fluid solution. Evidence for the participation of two excited states. *Inorg. Chem.* **1983**, *22*, 2380-2384.
(12) Ruthkosky, M.; Kelly, C. A.; Castellano, F. N.; Meyer, G. J. Electron and energy transfer from CuI MLCT excited states. *Coord. Chem. Rev.* **1998**, *171*, 309-322.
(13) Kern, J.-M.; Sauvage, J.-P. Photoassisted C-C coupling via electron transfer to benzylic halides by a bis(di-imine) copper(I) complex. *J. Chem. Soc. Chem. Commun.* **1987**, 546-548.
(14) Sandroni, M.; Maufroy, A.; Rebarz, M.; Pellegrin, Y.; Blart, E.; Ruckebusch, C.; Poizat, O.; Sliwa, M.; Odobel, F. Design of Efficient Photoinduced Charge Separation in Donor–Copper(I)–Acceptor Triad. *J. Phys. Chem. C* **2014**, *118*, 28388-28400; Barnsley, J. E.; Scottwell, S. O.; Elliott, A. B. S.; Gordon, K. C.; Crowley, J. D. Structural, Electronic, and Computational Studies of Heteroleptic Cu(I) Complexes of 6,6'-Dimesityl-2,2'-bipyridine with Ferrocene-Appended Ethynyl-2,2'-bipyridine Ligands. *Inorg. Chem.* **2016**, *55*, 8184-8192; Lazorski, M. S.; Gest, R. H.; Elliott, C. M. Photoinduced Multistep Charge Separation in a Heteroleptic Cu(I) Bis(phenanthroline)-Based Donor–Chromophore–Acceptor Triad. *J. Am. Chem. Soc.* **2012**, *134*, 17466-17469; Sandroni, M.; Favereau, L.; Planchat, A.; Akdas-Kilig, H.; Szuwarski, N.; Pellegrin, Y.; Blart, E.; Le Bozec, H.; Boujtita, M.; Odobel, F. Heteroleptic copper(i)-

polypyridine complexes as efficient sensitizers for dye sensitized solar cells. *J. Mater. Chem. A* **2014**, *2*, 9944-9947.
(15) Green, O.; Gandhi, B. A.; Burstyn, J. N. Photophysical Characteristics and Reactivity of Bis(2,9-di-tert-butyl-1,10-phenanthroline)copper(I). *Inorg. Chem.* **2009**, *48*, 5704-5714.
(16) Cunningham, C. T.; Cunningham, K. L. H.; Michalec, J. F.; McMillin, D. R. Cooperative Substituent Effects on the Excited States of Copper Phenanthrolines. *Inorg. Chem.* **1999**, *38*, 4388-4392.
(17) Eggleston, M. K.; McMillin, D. R.; Koenig, K. S.; Pallenberg, A. J. Steric Effects in the Ground and Excited States of Cu(NN)2+ Systems. *Inorg. Chem.* **1997**, *36*, 172-176.
(18) Agena, A.; Iuchi, S.; Higashi, M. Theoretical study on photoexcitation dynamics of a bis-diimine Cu(I) complex in solutions. *Chem. Phys. Chem.* **2017**, *679*, 60-65; McMillin, D. R.; Kirchhoff, J. R.; Goodwin, K. V. EXCIPLEX QUENCHING OF PHOTO-EXCITED COPPER-COMPLEXES. *Coord. Chem. Rev.* **1985**, *64*, 83-92.
(19) Dietrich-Buchecker, C. O.; Marnot, P. A.; Sauvage, J.-P.; Kirchhoff, J. R.; McMillin, D. R. Bis(2,9-diphenyl-1,10-phenanthroline)copper(I): a copper complex with a long-lived charge-transfer excited state. *J. Chem. Soc. Chem. Commun.* **1983**, 513-515; Pallenberg, A. J.; Koenig, K. S.; Barnhart, D. M. Synthesis and Characterization of Some Copper(I) Phenanthroline Complexes. *Inorg. Chem.* **1995**, *34*, 2833-2840.
(20) Mara, M. W.; Fransted, K. A.; Chen, L. X. Interplays of excited state structures and dynamics in copper(I) diimine complexes: Implications and perspectives. *Coord. Chem. Rev.* **2015**, *282–283*, 2-18; Lavie-Cambot, A.; Cantuel, M.; Leydet, Y.; Jonusauskas, G.; Bassani, D. M.; McClenaghan, N. D. Improving the photophysical properties of copper(I) bis(phenanthroline) complexes. *Coord. Chem. Rev.* **2008**, *252*, 2572-2584; Lazorski, M. S.; Castellano, F. N. Advances in the light conversion properties of Cu(I)-based photosensitizers. *Polyhedron* **2014**, *82*, 57-70.
(21) Garakyaraghi, S.; Crapps, P. D.; McCusker, C. E.; Castellano, F. N. Cuprous Phenanthroline MLCT Chromophore Featuring Synthetically Tailored Photophysics. *Inorg. Chem.* **2016**, *55*, 10628-10636.
(22) McCusker, C. E.; Castellano, F. N. Design of a Long-Lifetime, Earth-Abundant, Aqueous Compatible Cu(I) Photosensitizer Using Cooperative Steric Effects. *Inorg. Chem.* **2013**, *52*, 8114-8120.
(23) Gothard, N. A.; Mara, M. W.; Huang, J.; Szarko, J. M.; Rolczynski, B.; Lockard, J. V.; Chen, L. X. Strong Steric Hindrance Effect on Excited State Structural Dynamics of Cu(I) Diimine Complexes. *J. Phys. Chem. A* **2012**, *116*, 1984-1992.
(24) Arora, J. S.; Gaikar, V. G. Molecular design of a novel ligand for Menshutkin complexation of Bi(III) from aqueous acidic copper sulfate electrolyte solutions and experimental investigations. *RSC Adv.* **2016**, *6*, 39663-39674; Li, H.; Zhang, S.-G.; Xie, L.-M.; Yu, L.; Shi, J.-M. π-π Stacking and magnetic coupling mechanism on a mononuclear Cu(II) complex. *J. Coord. Chem.* **2011**, *64*, 3595-3608; Niu, C. Y.; Zheng, X. F.; Dang, Y. L. Dichlorido(2,9-dipropoxy-1,10-phenanthroline-κ2N,N')cadmium(II). *Acta Crystallogr., Sect. E: Struct. Rep. Online* **2009**, *65*, m1245; Albrecht-Gary, A. M.; Saad, Z.; Dietrich-Buchecker, C. O.; Sauvage, J. P. Interlocked macrocyclic ligands: a kinetic catenand effect in copper(I) complexes. *J. Am. Chem. Soc.* **1985**, *107*, 3205-3209.
(25) Bijloo, G. J.; Van der Goot, H.; Bast, A.; Timmerman, H. Copper complexes of 1,10-phenanthroline and related compounds as superoxide dismutase mimetics. *J. Inorg. Biochem.* **1990**, *40*, 237-244.
(26) Krapcho, A. P.; Sparapani, S.; Leenstra, A.; Seitz, J. D. Displacement reactions of 2-chloro- and 2,9-dichloro-1,10-phenanthroline: synthesis of a sulfur-bridged bis-1,10-phenanthroline macrocycle and a 2,2'-amino-substituted-bis-1,10-phenanthroline. *Tetrahedron Lett.* **2009**, *50*, 3195-3197; Hunziker, M.; Hauser, U. New 1,10-phenanthrolinethiols. *Heterocycles* **1982**, *19*, 2131-2138; Panda, K.; Siddiqui, I.; Mahata, P. K.; Ila, H.; Junjappa, H. Heteroannulation of 3-bis(methylthio)acrolein with aromatic amines - a convenient highly regioselective synthesis of 2-(methylthio)quinolines and their benzo/hetero fused analogs - a modified skraup quinoline synthesis. *Synlett* **2004**, 449-452.
(27) Wang, W.-J.; Sengul, A.; Luo, C.-F.; Kao, H.-C.; Cheng, Y.-H. Facile one-step synthesis of a thia-bridged bis-1,10-phenanthroline macrocycle. *Tetrahedron Lett.* **2003**, *44*, 7099-7101; Li, J.; Matsumoto, J.; Bai, L.-P.; Murata, A.; Dohno, C.; Nakatani, K. A Ligand That Targets CUG Trinucleotide Repeats. *Chem. Eur. J.* **2016**, *22*, 14761-14761.

(28) Borisova, N. E.; Kharcheva, A. V.; Patsaeva, S. V.; Korotkov, L. A.; Bakaev, S.; Reshetova, M. D.; Lyssenko, K. A.; Belova, E. V.; Myasoedov, B. F. Hard-and-soft phosphinoxide receptors for f-element binding: structure and photophysical properties of europium(iii) complexes. *Dalton. Trans.* **2017**, *46*, 2238-2248.
(29) Dehaudt, J.; Williams, N. J.; Shkrob, I. A.; Luo, H.; Dai, S. Selective separation of trivalent f-ions using 1,10-phenanthroline-2,9-dicarboxamide ligands in ionic liquids. *Dalton. Trans.* **2016**, *45*, 11624-11627.
(30) Liu, B.; Pan, S.; Liu, B.; Chen, W. Di-, Tri-, and Tetranuclear Copper(I) Complexes of Phenanthroline-Linked Dicarbene Ligands. *Inorg. Chem.* **2014**, *53*, 10485-10497.
(31) Keller, S.; Prescimone, A.; Bolink, H.; Sessolo, M.; Longo, G.; Martínez-Sarti, L.; Junquera-Hernández, J. M.; Constable, E. C.; Ortí, E.; Housecroft, C. E. Luminescent copper(i) complexes with bisphosphane and halogen-substituted 2,2′-bipyridine ligands. *Dalton. Trans.* **2018**, *47*, 14263-14276.
(32) Atkins, C. E.; Park, S. E.; Blaszak, J. A.; McMillin, D. R. A two-level approach to deconvoluting absorbance data involving multiple species. Applications to copper systems. *Inorg. Chem.* **1984**, *23*, 569-572.
(33) Attilio, A. G.; Michela, B.; Stefano, B.; Bruno, T. A Quantitative Description of the σ-Donor and π-Acceptor Properties of Substituted Phenanthrolines. *Eur. J. Inorg. Chem.* **2016**, *2016*, 3829-3837; Bessel, C. A.; Margarucci, J. A.; Acquaye, J. H.; Rubino, R. S.; Crandall, J.; Jircitano, A. J.; Takeuchi, K. J. Steric ligand effects of six bidentate bipyridyl ligands. *Inorg. Chem.* **1993**, *32*, 5779-5784.
(34) Cunningham, K. L.; McMillin, D. R. Reductive Quenching of Photoexcited Cu(dipp)2+ and Cu(tptap)2+ by Ferrocenes (dipp = 2,9-Diisopropyl-1,10-phenanthroline and tptap = 2,3,6,7-Tetraphenyl-1,4,5,8-tetraazaphenanthrene). *Inorg. Chem.* **1998**, *37*, 4114-4119.
(35) Miller, M. T.; Gantzel, P. K.; Karpishin, T. B. Effects of Sterics and Electronic Delocalization on the Photophysical, Structural, and Electrochemical Properties of 2,9-Disubstituted 1,10-Phenanthroline Copper(I) Complexes. *Inorg. chem.* **1999**, *38*, 3414-3422.
(36) Soulis, K.; Gourlaouen, C.; Daniel, C.; Quatela, A.; Odobel, F.; Blart, E.; Pellegrin, Y. New luminescent copper(I) complexes with extended π-conjugation. *Polyhedron* **2018**, *140*, 42-50.
(37)Arnold, D. R.; Baird, N. C.; Bolton, J. R.; Brand, J. C. D.; Jacobs, P. W. M.; DeMayo, P.; Ware, W. R. *Photochemistry: An Introduction*; Academic, 1974.
(38) Czerwieniec, R.; Leitl, M. J.; Homeier, H. H. H.; Yersin, H. Cu(I) complexes – Thermally activated delayed fluorescence. Photophysical approach and material design. *Coord. Chem. Rev.* **2016**, *325*, 2-28.
(39) Everly, R. M.; McMillin, D. R. Reinvestigation of the absorbing and emitting charge-transfer excited states of [Cu(NN)2]+ systems. *J. Phys. Chem.* **1991**, *95*, 9071-9075; Felder, D.; Nierengarten, J. F.; Barigelletti, F.; Ventura, B.; Armaroli, N. Highly luminescent Cu(I)-phenanthroline complexes in rigid matrix and temperature dependence of the photophysical properties. *J. Am. Chem. Soc.* **2001**, *123*, 6291-6299.
(40) Chen, L. X.; Shaw, G. B.; Novozhilova, I.; Liu, T.; Jennings, G.; Attenkofer, K.; Meyer, G. J.; Coppens, P. MLCT State Structure and Dynamics of a Copper(I) Diimine Complex Characterized by Pump−Probe X-ray and Laser Spectroscopies and DFT Calculations. *J. Am. Chem. Soc.* **2003**, *125*, 7022-7034.
(41) Iwamura, M.; Takeuchi, S.; Tahara, T. Real-Time Observation of the Photoinduced Structural Change of Bis(2,9-dimethyl-1,10-phenanthroline)copper(I) by Femtosecond Fluorescence Spectroscopy: A Realistic Potential Curve of the Jahn−Teller Distortion. *J. Am. Chem. Soc.* **2007**, *129*, 5248-5256; Iwamura, M.; Takeuchi, S.; Tahara, T. Ultrafast Excited-State Dynamics of Copper(I) Complexes. *Acc. Chem. Res.* **2015**, *48*, 782-791.
(42) Iwamura, M.; Watanabe, H.; Ishii, K.; Takeuchi, S.; Tahara, T. Coherent Nuclear Dynamics in Ultrafast Photoinduced Structural Change of Bis(diimine)copper(I) Complex. *J. Am. Chem. Soc.* **2011**, *133*, 7728-7736.
(43) Shaw, G. B.; Grant, C. D.; Shirota, H.; Castner, E. W.; Meyer, G. J.; Chen, L. X. Ultrafast Structural Rearrangements in the MLCT Excited State for Copper(I) bis-Phenanthrolines in Solution. *J. Am. Chem. Soc.* **2007**, *129*, 2147-2160.

(44) Garakyaraghi, S.; Danilov, E. O.; McCusker, C. E.; Castellano, F. N. Transient Absorption Dynamics of Sterically Congested Cu(I) MLCT Excited States. *J. Phys. Chem. A* **2015**, *119*, 3181-3193.
(45) Parker, W. L.; Crosby, G. A. Assignment of the charge-transfer excited states of bis(N-heterocyclic) complexes of copper(I). *J. Phys. Chem.* **1989**, *93*, 5692-5696.
(46) Phifer, C. C.; McMillin, D. R. The basis of aryl substituent effects on charge-transfer absorption intensities. *Inorg. Chem.* **1986**, *25*, 1329-1333.
(47) Smolentsev, G.; Soldatov, A. V.; Chen, L. X. Three-Dimensional Local Structure of Photoexcited Cu Diimine Complex Refined by Quantitative XANES Analysis. *J. Phys. Chem. A* **2008**, *112*, 5363-5367.
(48) Siddique, Z. A.; Yamamoto, Y.; Ohno, T.; Nozaki, K. Structure-Dependent Photophysical Properties of Singlet and Triplet Metal-to-Ligand Charge Transfer States in Copper(I) Bis(diimine) Compounds. *Inorg. Chem.* **2003**, *42*, 6366-6378.
(49) Samanta, P. K.; Kim, D.; Coropceanu, V.; Brédas, J.-L. Up-Conversion Intersystem Crossing Rates in Organic Emitters for Thermally Activated Delayed Fluorescence: Impact of the Nature of Singlet vs Triplet Excited States. *J. Am. Chem. Soc.* **2017**, *139*, 4042-4051.
(50) Penfold, T. J.; Gindensperger, E.; Daniel, C.; Marian, C. M. Spin-Vibronic Mechanism for Intersystem Crossing. *Chem. Rev.* **2018**, *118*, 6975-7025.
(51) Stoïanov, A.; Gourlaouen, C.; Vela, S.; Daniel, C. Luminescent Dinuclear Copper(I) Complexes as Potential Thermally Activated Delayed Fluorescence (TADF) Emitters: A Theoretical Study. *J. Phys. Chem. A* **2018**, *122*, 1413-1421.
(52) Capano, G.; Penfold, T. J.; Röthlisberger, U.; Tavernelli, I. A Vibronic Coupling Hamiltonian to Describe the Ultrafast Excited State Dynamics of a Cu(I)-Phenanthroline Complex. *CHIMIA International Journal for Chemistry* **2014**, *68*, 227-230; Capano, G.; Rothlisberger, U.; Tavernelli, I.; Penfold, T. J. Theoretical Rationalization of the Emission Properties of Prototypical Cu(I)–Phenanthroline Complexes. *J. Phys. Chem. A* **2015**, *119*, 7026-7037; Föller, J.; Kleinschmidt, M.; Marian, C. M. Phosphorescence or Thermally Activated Delayed Fluorescence? Intersystem Crossing and Radiative Rate Constants of a Three-Coordinate Copper(I) Complex Determined by Quantum-Chemical Methods. *Inorg. Chem.* **2016**, *55*, 7508-7516; Penfold, T. J.; Karlsson, S.; Capano, G.; Lima, F. A.; Rittmann, J.; Reinhard, M.; Rittmann-Frank, M. H.; Braem, O.; Baranoff, E.; Abela, R.; Tavernelli, I.; Rothlisberger, U.; Milne, C. J.; Chergui, M. Solvent-Induced Luminescence Quenching: Static and Time-Resolved X-Ray Absorption Spectroscopy of a Copper(I) Phenanthroline Complex. *J. Phys. Chem. A* **2013**, *117*, 4591-4601.
(53) Oszlanyi, G.; Suto, A. Ab initio structure solution by charge flipping. *Acta Crystallogr. A* **2004**, *60*, 134-141.
(54) Palatinus, L.; Chapuis, G. SUPERFLIP - a computer program for the solution of crystal structures by charge flipping in arbitrary dimensions. *J. Appl. Cryst.* **2007**, *40*, 786-790.
(55)Petricek, V.; Dusek, M.; Palatinus, L.; Institute of Physics, Praha, Czech Republic: 2006.
(56) Stephens, P. J.; Devlin, F. J.; Chabalowski, C. F.; Frisch, M. J. Ab Initio Calculation of Vibrational Absorption and Circular Dichroism Spectra Using Density Functional Force Fields. *J. Phys. Chem.* **1994**, *98*, 11623-11627.
(57) Van Lenthe, E.; Baerends, E. J. Optimized Slater-type basis sets for the elements 1–118. *J. Comput. Chem.* **2003**, *24*, 1142-1156.
(58) Grimme, S.; Antony, J.; Ehrlich, S.; Krieg, H. A consistent and accurate ab initio parametrization of density functional dispersion correction (DFT-D) for the 94 elements H-Pu. *J. Chem. Phys.* **2010**, *132*.
(59) E., v. L.; R., v. L.; J., B. E.; G., S. J. Relativistic regular two ‐ component Hamiltonians. *Int. J. Quantum. Chem.* **1996**, *57*, 281-293.
(60) Klamt, A. Conductor-like Screening Model for Real Solvents: A New Approach to the Quantitative Calculation of Solvation Phenomena. *J. Phys. Chem.* **1995**, *99*, 2224-2235; Klamt, A.; Jonas, V. Treatment of the outlying charge in continuum solvation models. *J. Chem. Phys.* **1996**, *105*, 9972-9981; Klamt, A.; Schuurmann, G. COSMO - A NEW APPROACH TO DIELECTRIC SCREENING IN SOLVENTS WITH EXPLICIT EXPRESSIONS FOR THE SCREENING ENERGY AND ITS GRADIENT. *J. Chem. Soc. Perkin Trans. 2* **1993**, 799-805.

(61) Peach, M. J. G.; Tozer, D. J. Overcoming Low Orbital Overlap and Triplet Instability Problems in TDDFT. *J. Phys. Chem. A* **2012**, *116*, 9783-9789.
(62) Wang, F.; Ziegler, T. A simplified relativistic time-dependent density-functional theory formalism for the calculations of excitation energies including spin-orbit coupling effect. *The Journal of Chemical Physics* **2005**, *123*, 154102; Wang, F.; Ziegler, T.; van Lenthe, E.; van Gisbergen, S.; Baerends, E. J. The calculation of excitation energies based on the relativistic two-component zeroth-order regular approximation and time-dependent density-functional with full use of symmetry. *J. Chem. Phys.* **2005**, *122*.
(63) Perdew, J. P.; Burke, K.; Ernzerhof, M. Generalized gradient approximation made simple. *Phys. Rev. Lett.* **1996**, *77*, 3865-3868; Perdew, J. P.; Burke, K.; Ernzerhof, M. Generalized gradient approximation made simple (vol 77, pg 3865, 1996). *Phys. Rev. Lett.* **1997**, *78*, 1396-1396.
(64) Grimme, S. Semiempirical GGA-type density functional constructed with a long-range dispersion correction. *J. Comput. Chem.* **2006**, *27*, 1787-1799.
(65) Vanderbilt, D. Soft self-consistent pseudopotentials in a generalized eigenvalue formalism. *Phys. Rev. B* **1990**, *41*, 7892-7895.
(66) Berendsen, H. J. C.; Postma, J. P. M.; Vangunsteren, W. F.; Dinola, A.; Haak, J. R. MOLECULAR-DYNAMICS WITH COUPLING TO AN EXTERNAL BATH. *J. Chem. Phys.* **1984**, *81*, 3684-3690.
(67) Makov, G.; Payne, M. C. PERIODIC BOUNDARY-CONDITIONS IN AB-INITIO CALCULATIONS. *Phys. Rev. B* **1995**, *51*, 4014-4022.
(68) Giannozzi, P.; Baroni, S.; Bonini, N.; Calandra, M.; Car, R.; Cavazzoni, C.; Ceresoli, D.; Chiarotti, G. L.; Cococcioni, M.; Dabo, I.; Dal Corso, A.; de Gironcoli, S.; Fabris, S.; Fratesi, G.; Gebauer, R.; Gerstmann, U.; Gougoussis, C.; Kokalj, A.; Lazzeri, M.; Martin-Samos, L.; Marzari, N.; Mauri, F.; Mazzarello, R.; Paolini, S.; Pasquarello, A.; Paulatto, L.; Sbraccia, C.; Scandolo, S.; Sclauzero, G.; Seitsonen, A. P.; Smogunov, A.; Umari, P.; Wentzcovitch, R. M. QUANTUM ESPRESSO: a modular and open-source software project for quantum simulations of materials. *J. Phys. Condens. Matter* **2009**, *21*.
(69) Frey, J.; Kraus, T.; Heitz, V.; Sauvage, J.-P. Synthesis of a Bis-macrocycle Containing Two Back-to-Back Rigidly Connected 1,10-Phenanthroline Units as a Central Core and its Incorporation in a Handcuff-Like Catenane. *Chem. Eur. J.* **2007**, *13*, 7584-7594.
(70) Ogawa, S.; Yamaguchi, T.; Gotoh, N. Preparation of a conjugated tautomer of 1,14:7,8-diethenotetrapyrido-[2,1,6-de:2[prime or minute],1[prime or minute],6[prime or minute]-gh:2[double prime],1[double prime],6[double prime]-kl:2[triple prime],1[triple prime],6[triple prime]na][1,3,5,8,10,12]hexa-azacyclotetradecine and its metal derivatives. *J. Chem. Soc. Perkin Trans. 1* **1974**, 976-978.
(71) Kubas, G. J. Tetrakis(acetonitrile)copper(I) hexafluorophosphate. *Inorg. Synth.* **1979**, *19*, 90-92.